Arctic Ocean primary production from 1980-2015: Implications of biogeochemical model parameterizations

Nadja Steiner, Jim Christian, Olivier Riche, Tessa Sou

Fisheries and Oceans Canada
Science Branch,
Pacific Region
Institute of Ocean Sciences
P.O. Box 6000
Sidney, B.C. V8L 4B2
Nadja.Steiner@dfo-mpo.gc.ca

2024

Canadian Technical Report of
Fisheries and Aquatic Sciences 3561

Fisheries and Oceans Canada | Pêches et Océans Canada

Canada

Canadian Technical Report of Fisheries and Aquatic Sciences

Technical reports contain scientific and technical information that contributes to existing knowledge but which is not normally appropriate for primary literature. Technical reports are directed primarily toward a worldwide audience and have an international distribution. No restriction is placed on subject matter and the series reflects the broad interests and policies of Fisheries and Oceans Canada, namely, fisheries and aquatic sciences.

Technical reports may be cited as full publications. The correct citation appears above the abstract of each report. Each report is abstracted in the data base *Aquatic Sciences and Fisheries Abstracts*.

Technical reports are produced regionally but are numbered nationally. Requests for individual reports will be filled by the issuing establishment listed on the front cover and title page.

Numbers 1-456 in this series were issued as Technical Reports of the Fisheries Research Board of Canada. Numbers 457-714 were issued as Department of the Environment, Fisheries and Marine Service, Research and Development Directorate Technical Reports. Numbers 715-924 were issued as Department of Fisheries and Environment, Fisheries and Marine Service Technical Reports. The current series name was changed with report number 925.

Rapport technique canadien des sciences halieutiques et aquatiques

Les rapports techniques contiennent des renseignements scientifiques et techniques qui constituent une contribution aux connaissances actuelles, mais qui ne sont pas normalement appropriés pour la publication dans un journal scientifique. Les rapports techniques sont destinés essentiellement à un public international et ils sont distribués à cet échelon. II n'y a aucune restriction quant au sujet; de fait, la série reflète la vaste gamme des intérêts et des politiques de Pêches et Océans Canada, c'est-à-dire les sciences halieutiques et aquatiques.

Les rapports techniques peuvent être cités comme des publications à part entière. Le titre exact figure au-dessus du résumé de chaque rapport. Les rapports techniques sont résumés dans la base de données *Résumés des sciences aquatiques et halieutiques.*

Les rapports techniques sont produits à l'échelon régional, mais numérotés à l'échelon national. Les demandes de rapports seront satisfaites par l'établissement auteur dont le nom figure sur la couverture et la page du titre.

Les numéros 1 à 456 de cette série ont été publiés à titre de Rapports techniques de l'Office des recherches sur les pêcheries du Canada. Les numéros 457 à 714 sont parus à titre de Rapports techniques de la Direction générale de la recherche et du développement, Service des pêches et de la mer, ministère de l'Environnement. Les numéros 715 à 924 ont été publiés à titre de Rapports techniques du Service des pêches et de la mer, ministère des Pêches et de l'Environnement. Le nom actuel de la série a été établi lors de la parution du numéro 925.

Canadian Technical Report of
Fisheries and Aquatic Sciences 3561

2024

Arctic Ocean primary production from 1980-2015: Implications of biogeochemical model parameterizations

by

Nadja Steiner[1], Jim Christian[1], Olivier Riche[2], Tessa Sou[1]

[1] Fisheries and Oceans Canada, Institute of Ocean Sciences Sidney, BC
[2] Fisheries and Oceans Canada, Maurice Lamontagne Institute Mont-Joli, QC

Cat. No. Fs 97-6/3561E-PDF ISBN 978-0-660-67763-7 ISSN 1488-5379

Correct citation for this publication:

Steiner, N., Christian, J., Riche, O., Sou, T. 2024. Arctic Ocean primary production from 1980-2015: Implications of biogeochemical model parameterizations. Can. Tech. Rep. Fish. Aquat. Sci. 3561: v + 45 p.

Table of Contents

ABSTRACT

Steiner, N., Christian, J., Riche, O., Sou, T. 2023. Arctic Ocean primary production from 1980-2015: Implications of biogeochemical model parameterizations. Can. Tech. Rep. Fish. Aquat. Sci. 3561: v + 45 p.

Modelling studies addressing the spatial and temporal evolution of Arctic primary production (PP) show large differences among models. These differences affect the credibility of climate projections and our ability to assess impacts on higher trophic level species. Model intercomparisons have shown that many differences in biogeochemical outputs are related to the models' physical fields, e.g., ice and snow coverage (impacting light), and water column stratification (impacting nutrient supply). Here, we evaluate three biogeochemical models within the same 3D physical ocean-ice-snow model of the Arctic. We evaluate simulated trends and regional averages of PP and vertical patterns of chlorophyll-a (Chla) concentrations over the time period 1980-2015 and augment the analysis with sensitivity studies in a 1-D model framework. Results indicate that different biogeochemical parameterizations affect the seasonal evolution and vertical structure of the primary producers, including the evolution of the subsurface deep Chla maximum (SCM). Key model differences driving the SCM are: 1. The treatment of dissolved inorganic nitrogen and its uptake by phytoplankton; 2. the phytoplankton light attenuation; and 3. the application of multiple detrital sinking rates in higher complexity models. Annual regional-mean vertically integrated PP, long term trends and large-scale regional variability in PP show less sensitivity to the choice of the biogeochemical model, providing some confidence in our ability to project total PP changes in future scenarios.

RÉSUMÉ

Steiner, N., Christian, J., Riche, O., Sou, T. 2023. Arctic Ocean primary production from 1980-2015: Implications of biogeochemical model parameterizations. Can. Tech. Rep. Fish. Aquat. Sci. 3561: v + 45 p.

Des études précédentes de modélisation portant sur l'évolution spatio-temporelle de la production primaire (PP) dans l'Arctique ont montré de grandes différences entre les modèles. Ces différences affectent la crédibilité des projections climatiques et notre capacité à évaluer les impacts sur les espèces de niveau trophique supérieur. Les comparaisons inter-modèles ont montré que de nombreuses différences dans la production biogéochimique sont liées aux champs physiques des modèles, tels que la couverture de glace et de neige (impact de la lumière) et la stratification de la colonne d'eau (impact sur l'approvisionnement en nutriments). Ici, nous supprimons l'impact de différents champs physiques en évaluant trois modèles biogéochimiques dans le même modèle physique 3D océan-glace-neige de l'Arctique. Nous évaluons les tendances simulées et les moyennes régionales de la PP arctique et les patrons verticaux des concentrations de chlorophylle-a (Chla) sur la période 1980-2015 et ajoutons à l'analyse des études de sensibilité dans une plateforme de modélisation 1D. Les résultats indiquent que différentes paramétrisations affectent l'évolution saisonnière et la structure verticale des producteurs primaires, y compris l'évolution du maximum de Chla profond sous la surface (SCM). Les principales différences en simulée du SCM sont : 1. Le traitement de l'azote inorganique dissous et son utilisation par le phytoplancton; 2. l'atténuation de la lumière du phytoplancton; et 3. l'application de multiples taux de chute détritiques dans des modèles de complexité plus élevée. La moyenne annuelle de la PP verticalement intégrée, les tendances à long terme et la variabilité régionale à grande échelle de la PP montrent une moindre sensibilité au choix du modèle biogéochimique. Cela donne une certaine confiance dans notre capacité à prévoir les changements totaux de la PP dans les scénarios futurs.

1. INTRODUCTION

Primary producers, such as pelagic (oceanic) phytoplankton and sea-ice algae, represent the base of the food chain in the Arctic ocean. In general ecology, gross primary production (PP) refers to the synthesis of organic compounds from carbon dioxide and defines the amount of chemical energy as biomass that primary producers create in each length of time, net PP refers to the rate at which photosynthesis occurs. Hence, PP within an ecosystem provides a measure of how much energy and biomass is available for transfer to higher trophic level (HTL) species. Understanding the interannual variability and long-term trends in Arctic PP is therefore relevant for the understanding of HTL species impacts.

Modelling studies assessing the spatial and temporal evolution of Arctic PP show large differences among models [e.g., Popova et al., 2012; Vancoppenolle et al., 2013; Steiner et al., 2015; Lee et al., 2015; Jin et al., 2016; Hayashida et al., 2019]. These differences call into question our ability to project long-term climate change impacts on Arctic marine ecosystems as well as shorter term forecasts. Previous modelling studies (cited above) highlight the importance of ocean and sea-ice processes in the simulation of biogeochemical fields. Vertical mixing, horizontal advection, and ocean stratification impact nutrient distributions; sea-ice thickness and coverage impact the light availability to the ocean.

In this study, differences in the ocean-ice field are removed by running different biogeochemical models within the same physical model (ocean, sea ice and snow and associated setup and forcing) to evaluate 1. how the models differ in their representation of the vertical pattern and evolution of PP, Chla and phytoplankton concentration, 2. if model differences affect our ability to simulate long-term trends in primary production, and 3. what causes the differences and if they can be remediated with model tuning. To address the latter, additional sensitivity studies were performed within a 1-D model framework.

While PP is readily available from modelling studies, observations are very limited and often only phytoplankton concentration or Chla is measured. Phytoplankton concentration and chlorophyll-a (Chla) are both measures of biomass present at a specific time. The same concentrations can be measured in a system with low PP and low loss terms (e.g., zooplankton grazing, mortality) and by a system with high PP and high loss terms. Hence, PP and phytoplankton or Chla concentrations are not interchangeable. Models simulate PP in units of C over a specified area, depth, and time. Phytoplankton concentrations are usually given in units of carbon or nitrogen in a given volume which can then be converted into Chla concentrations via constant or variable N:Chla or C:Chla ratios. Given the sparsity of available observation for any of the variables (PP, phytoplankton concentrations, and Chla), all were used to evaluate model performance.

With respect to the vertical pattern of Chla (and phytoplankton concentrations), the Arctic Ocean exhibits a characteristic feature which is referred to as the subsurface Chla maximum (SCM). The SCM develops seasonally during the post-bloom period when near-surface nutrients have been depleted by phytoplankton. Phytoplankton then move deeper into the water column where light and nutrients still provide conditions suitable for growth. The SCM can contribute significantly to the vertically integrated Chla concentration, even though no Chla may be observed at the surface [e.g., Ardyna et al., 2013]. The correct representation of the pattern (timing and depth) of the SCM is dependent on a balance of phytoplankton primary production, nutrients, and light. The reproduction of this characteristic feature in biogeochemical models can be used as an indicator for model performance. Steiner et al. [2015] evaluated the simulated SCM in several models and found that inter-model differences in the reproduction of the SCM are mainly linked to inconsistencies in nutrient availability and differences in the represented ecosystem community structure among the models, while differences in the depth of an existing SCM are likely caused by a variety of physical factors such as the rate of sea ice retreat,

strength of the Beaufort Gyre circulation, and horizontal water mass transport. In addition, Hayashida et al. [2019] highlighted that adopting a high vertical resolution in the upper water column improves the representation of a surface meltwater lens, its effects on surface nutrients and the formation of a SCM.

2. BACKGROUND AND METHODS

2.1. Biogeochemical Models

The North Atlantic-Arctic (NAA) physical model is executed with a selection of biogeochemical modules. Our main focus is the comparison of the Canadian Ocean Ecosystem model (CanOE), a version of CanOE coupled to the Canadian sea-ice biogeochemistry model (CanOE-CSIB), and the Canadian Model for Ocean Carbon (CMOC). The Pelagic Interactions Scheme for Carbon and Ecosystem Studies (PISCES) model is one of the base biogeochemical models included in the Nucleus for European Modelling of the Ocean (NEMO) system and is included in some of the evaluations. In a spectrum of increasing complexity of the biogeochemical processes and the marine ecosystem, CMOC is the simplest followed by CanOE and PISCES.

2.1.1. The Canadian Ocean Ecosystem model (CanOE)

CanOE includes the two nutrient compartments nitrate (NO_3^-, hereafter NO3) and ammonium (NH_4^+, hereafter NH4) and two (small and large) compartments each for phytoplankton, zooplankton, and detritus, with a total of seventeen tracers, including dissolved inorganic carbon (DIC), total alkalinity (TA), and oxygen. Note, CanOE generally also includes Fe, however Fe dependence is not activated in the current Arctic version. It also has variable phytoplankton elemental ratios, where each element represents a separate tracer [Christian et al. 2022]. The separation of phytoplankton and zooplankton into multiple species in higher complexity models also allows for the separation of detrital pools, which can then be assigned different sinking speeds. This affects the location of nutrient (NO3 and NH4) remineralization and hence availability to the ecosystem. Nitrogen pathways are more complex in CanOE as both NO3 and NH4 are available and both contribute proportionally to phytoplankton growth. CanOE includes a phytoplankton NH4 preference, i.e., NO3 uptake is inhibited if enough NH4 is available. This inhibition can impact the depth where primary producers accumulate and the SCM develops. CanOE also has prognostic nitrification, denitrification (respiration of NO3 where ([O2] < 6 mmol m-3), and N2 fixation, but both denitrification and N2 fixation are negligible within the high-latitude NAA domain. Nitrification only happens in the dark and will be limited within the euphotic zone during polar summer. Global Earth System Model simulations with CanESM5-CanOE are available through the Coupled Model Intercomparison Project version 6 (CMIP6) [Swart et al 2019, Christian et al 2022]

2.1.2. The Canadian Sea Ice Biogeochemistry (CanOE-CSIB) model

CanOE is coupled to the Canadian Sea Ice Biogeochemistry model, CanOE-CSIB [Hayashida et al., 2019]. CSIB represents sea ice algae as an additional photosynthetic functional group, experiencing growth, mortality, and nutrient uptake. The simulated ice algae have a higher sensitivity to low-light conditions relative to pelagic phytoplankton and ice algae released from sea-ice contribute to the large detritus and the pelagic large phytoplankton pools (seeding) in CanOE [Mortenson et al., 2017; Hayashida et al., 2019].

2.1.3. The Canadian Model of Ocean Carbon (CMOC)

CMOC is a NPZD model with one species each of nutrient (N), phytoplankton (P),

Zooplankton (Z) and detritus (D) with fixed (Redfield) elemental ratios. Additional tracers include dissolved inorganic carbon (DIC), total alkalinity (TA) and Chla. Chla is calculated semi-prognostically using both a chlorophyll synthesis term and relaxation towards an irradiance-dependent Chla/C ratio [Zahariev et al., 2007]. The single N-compartment represents all dissolved inorganic nitrogen and denitrification is prescribed to balance nitrogen fixation within a single vertical column. Dissolved inorganic nitrogen is derived directly from the remineralization of organic particles (no dissolved organic matter component) and without speciation between NO3 and NH4 (nitrification is therefore not needed). CMOC was one of the earliest attempts to implement the full carbon cycle in an Earth System model [Arora et al, 2009; Christian et al 2010]. As a result, it is very simple compared to more recent models. CMOC continues to be used in the Canadian Earth System Model version 5 (CanESM5) which allows for the contribution of large ensembles to CMIP6) [Swart et al 2019, Christian et al 2022].

2.1.4. The Pelagic Interactions Scheme for Carbon and Ecosystem Studies (PISCES) model

PISCES [Aumont et al., 2015] has a total of 24 tracers and has a plankton community structure similar to CanOE but with fixed ratios for some elements. In addition to the two detritus pools, PISCES includes a dissolved organic matter pool and multiple nutrients (NO3, NH4, PO4, Si, Fe). There is no inhibition of NO3 uptake by NH4 in PISCES .

2.2. The 3-D Physical Model

The North Atlantic Arctic (NAA) regional ocean-sea ice model (Fig. 1) uses the Nucleus for European Modelling of the Oceans version 3.4 [NEMO, Madec, 2008] with the Louvain-la-Neuve sea Ice Model version 2 (LIM2) in the configuration of Hu and Myers [2013, 2014]. The horizontal grid resolution ranges from 10 km near the North American coastline to 14.5 km along the northern Eurasian coastline. The vertical resolution was modified from the original NAA configuration to have higher vertical resolution near the ocean surface (from 6 m for the upper surface layer to 1 m), as described in Hayashida [2018]. The timestep is 20 minutes. The default setting for LIM2 does not allow light penetration in the presence of snow. To allow adequate light penetration at the time of observed ice algae blooms, LIM2 was modified as described in Hayashida [2018]. This change is particularly relevant for adequate representation of early spring ice algae production and to some extent for late spring under-ice pelagic production. However, it has no impact on the phytoplankton evolution during the open water season when the SCM evolves (an example using NAA-CMOC is shown in Fig. S13, Appendix 2). The PISCES model has been run without the light penetration adjustment in LIM2, but as the impacts are extremely limited for the topic discussed here, this should not be an issue. The CMOC, CanOE-CSIB and PISCES runs were run from 1969-2015 with a spin-up period from 1969-1979. The CanOE model without CSIB has been run from 1990 to 2015 (Mortenson et al. 2020) as a sensitivity study to assess potential impacts of omitting sea-ice algal production on PP and Chla and has been assessed for the time period of 1995 to 2015. Additional model experiment details for reference are included in Appendix 2.

2.3. Forcing

For this study, the NAA model was forced by meteorological data for the Arctic Ocean for 1969 to 2015, using the Drakkar Forcing Set version 5.2 [DFS; Dussin et al., 2016]. The DFS dataset provides atmospheric information on a 0.7-degree resolution grid, with temporal resolution of 3 hours for winds (10 m above the surface) and air temperature and humidity (2 m); and daily resolution for incoming shortwave and longwave radiation, snowfall, and total precipitation (rain plus snow) All forcing data was interpolated to the 20min timestep. Coastal runoff and major river input was based on the climatological monthly means [Dai and Trenberth, 2002, Dai et al. 2009]. Nutrient concentrations were assigned to runoff only at the mouths of the six major Arctic

rivers (MacKenzie and Yukon Rivers in North America, and Kolyma, Lena, Yenisey, and Ob in Eurasia). Nutrient information was taken from multiple sources [Tank et al., 2012 (DIC), Cooper et al., 2008 (DOC, TA), and McClelland et al., 2012 (NO3)]. Dissolved organic nitrate (DON) was calculated from DON:DIN ratios from Holmes et al. [2012] with NO3 and Dissolved Inorganic Nitrogen (DIN) from McClelland et al. [2012] (see summary in Hayashida 2018, their table A.6). Because there is no DOC or DON in CanOE, river input of DOC and DON was added directly to the inorganic pools (DIC and NO3). Open-ocean boundaries of the model domain are in the Bering Sea (south of Bering Strait), and in the North Atlantic (south of Greenland). The ocean boundary conditions for physical variables (temperature, salinity, and velocity) are from climatological monthly mean fields of the operational ocean analysis/reanalysis system ORAS4 [Balmaseda et al., 2013], interpolated to the NAA grid. Relaxation time scales were set to 1 day for inflow and 15 days for outflow, consistent with Dupont et al. [2015]. DIC, TA and NO3 at the open-ocean boundaries are based on the annual mean climatology from GLODAPv2 and O2 is from the World Ocean Atlas [WOA13, Garçon et al., 2014].

2.4. The 1-D model

The general ocean turbulence model (GOTM) is a 1-D model tool which has been developed to study near surface processes. It is coupled to a sea-ice model [Abraham et al., 2015] as well as ocean and sea-ice biogeochemical models (GOTM-CSIB-1D) [Mortenson et al., 2017]. The model is well suited to perform sensitivity studies for single and multiple parameter changes. GOTM is run for the location of Resolute Bay on the Canadian Polar Shelf (CPS) (74ºN, 95ºW) for the spring to summer time period (year-days 150 to 270, i.e., end of May to September) with 2010 forcing as described in Mortenson et al. [2017]. To specifically explore the impacts within the CanOE model, the GOTM pelagic ecosystem in Mortenson et al. [2017] has been replaced with CanOE. A version with CMOC has also been set up for comparison.
Sensitivity studies with GOTM-CanOE using three different values for each chosen model parameter (Table 1) were performed for combinations of detrital sinking and phytoplankton growth rates, linear and quadratic phytoplankton mortality rates and for the initial slope of the PI curve to better understand how these parameters impact the seasonal evolution of Chla in the water column. Parameter values for the sensitivity studies are given in Table 1. The sensitivity experiments were performed without the ice algae component. Differences for simulations with and without sea-ice algae in GOTM were evaluated by Mortenson et al. [2017] and indicate higher near-surface Chla concentrations at the begin of the phytoplankton bloom for the no-ice algae run (due to increased nutrient availability for pelagic plankton without ice algae uptake), but a similar evolution of the SCM.

Table 1. Parameter Values for 1-D sensitivity studies

Rate Parameters	**Units**	**Value 1**	**Value 2**	**Value 3**
Sinking	m d^{-1}	1	8	10
Growth	d^{-1}	1.0	3.0	4.0
Linear mortality	mmol-C m^{-3} d^{-1}	0.0125, 0.0250	0.05, 0.101	0.2, 0.4
Quadratic mortality	mmol-C m^{-3} d^{-1}	0.02	0.06	0.18
P-I curve initial slope	mgC (mgChl-a)$^{-1}$ h^{-1} (µmol quanta m^{-2} s^{-1})$^{-1}$	0.8	1.3	1.73

2.5. Observations

In the Arctic, observations of PP, plankton and Chla concentrations are very sparse. A comprehensive compilation of Arctic PP and Chla, covering five decades, was provided in the ARCCSS-PP database [Matrai et al., 2013; Hill et al., 2013]. The dataset contains spatial and seasonal biases with large data gaps in almost all seasons, particularly for direct PP observations. Data availability is highest for July-August-September and for 1988-1997. Availability of Chla measurements is slightly higher and can be augmented by satellite Chla estimates. However, satellite observations in the Arctic can be prone to significant errors e.g., due to the development of SCMs [e.g., Ardyna et al., 2013]. Given the limited PP observations, spatial and temporal averages are used in the model evaluations. Matrai et al. [2013] and Hill et al. [2013] averaged and evaluated integrated PP (IPP, integrated over the euphotic layer) for 14 subregions in the Arctic which guided the regional subdivision applied here (Fig.1). Their estimates of PP depend on the sea-ice cover based on the HadISST sea-ice reanalysis dataset.

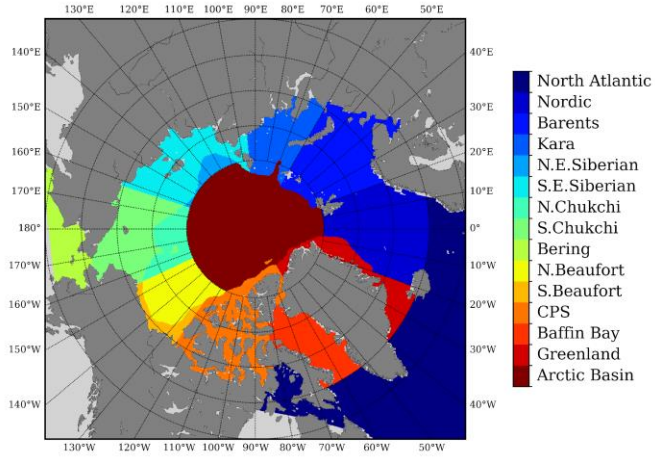

Figure 1: Subregion partitioning

Subregion partitioning of the NAA model following Matrai et al., [2013], with the exception of Baffin Bay which is treated as a separate region rather than split into Eastern and Western parts.

3. 3-D MODEL RESULTS

To assess the differences among biogeochemical models, we evaluated pan-Arctic and sub-regionally averaged PP, and the representation of a SCM in the Beaufort Sea and Canadian Polar Shelf, including along a transect line through the Canadian Polar Shelf, as well as past trends in PP and phytoplankton concentration .

3.1. Pan-Arctic Primary Production

A summary of observation and model-based annual estimates for Arctic PP is given in Table 2. Spring and summer seasonal averages by region are shown in supplementary Table S2, Appendix 3. Simulated net ocean PP over the pan-Arctic region (referring to the area north of 66.5ºN) CanOE-CSIB (525 Tg-C y^{-1}) and CMOC (613 Tg-C y^{-1}) PP are within the range given by satellite-based estimates from Arrigo and van Dijken [2015] and two other model results [Zhang et al., 2010; Watanabe et al., 2019]. The CanOE-CSIB mean agrees with that of Watanabe et al. [2019], while the CMOC mean is closer to the somewhat higher estimates of the model studies by Jin et al. 2012 and Popova et al., 2012. The simulated PP is approximately one half of earlier estimates based on in situ measurements by Sakshaug [2004]. Remote sensing estimates by Hill et al. [2013] estimate 466 Tg-C y^{-1} with about twice the amount (993 Tg-C y^{-1}) if they include estimated SCM production. Observation-based estimates are uncertain, primarily due to spatially and temporally limited observations. Note, other satellite estimates [Arrigo and van Dijken, 2011; Ardyna et al., 2013] regard the contribution of subsurface production to the pan-Arctic annual net PP as negligible. The ice algal contribution to the total (sea ice and ocean) net PP over the pan-Arctic is only 2.3 % in CanOE-CSIB and adds about 12 Tg-C y^{-1} to the total PP, which is in close agreement with previous model studies (1.8 % in Watanabe et al. [2019] and 1.6 % in Jin et al. [2012]). PISCES (244 Tg-C y^{-1}) shows less than half of the CanOE-CSIB and CMOC estimates and is below the expected range for annual net PP in the Arctic (Table 2).

Table 2. Comparison of pan-Arctic annual net primary production by pelagic phytoplankton.
The range and/or the mean 1 standard deviation (in square brackets) are quoted. Pan-Arctic refers to roughly the region north of 66.5º N.

Value (Tg-C y^{-1})	Method	Temporal Coverage	Reference
525	Model	1980-2015	NAA-CanOE-CSIB, this study
613	Model	1980-2015	NAA-CMOC, this study
224	Model	1980-2015	NAA-PISCES, this study
893	In situ measurements	Unknown	Sakshaug [2004]
466±94	Satellite	1998-2007	Hill et al. [2013]
993±94	Satellite plus SCM	1998-2007	Hill et al. [2013]
460-608	Satellite 1998-2012	1998-2012	Arrigo and van Dijken [2015]
456-682	Model	1988-2007	Zhang et al. [2010]
627±51	Model	1998-2007	Jin et al. [2012]
626±20	Model	1990-2006	Popova et al. [2012]
385-615 (503±57)	Model	1980-2013	Watanabe et al. [2019]

3.2. Regional Comparison of Vertically Integrated Primary Production

Evaluating vertically integrated primary production allows us to compare annual productivity and seasonal patterns among models, even though the vertical evolution and structure in the water column may be different. Fig. 2 shows IPP for CanOE-CSIB (cyan), CanOE (dark blue), CMOC (yellow) and PISCES (magenta) within the NAA model, compared to the observations [Hill et al., 2013, black] for twelve of the Arctic subregions indicated in Fig. 1. Note that the model results have been averaged from 1995 to 2010, while the observations [Hill et al., 2013] represent an average from 1954 to 2009 (with a majority of data points between 1988 and 1997). Comparing CanOE with CanOE-CSIB provides information on the contribution of sea-ice algae.
A few patterns emerge: 1) the models capture the main seasonal cycle in most regions, including a secondary late summer bloom in some regions (e.g., Barents Sea, Arctic Basin, Fig. 2 g, j); 2) CMOC and PISCES show lower PP and underestimate the observed values in most regions and months. 3) Sea-ice algae have a positive, but small effect on the pelagic primary

production. In most cases pelagic PP is slightly increased, this is likely related to the seeding effect ice algae have on pelagic plankton and near-surface nutrient remineralization, despite an initial reduction in phytoplankton concentration due to the uptake of nutrients by ice algae [e.g., Mortenson et al., 2017]. 4) The observations show occasional high peaks in PP which are not reproduced by any of the ecosystem models (e.g., CPS, Bering and Greenland Seas Fig. 2 a, d, k).

The observations are integrated over the euphotic layer and for regions with open water [Hill et al. 2013], where open water is defined as a cell with ice cover less than 50%. In the model, integration to the mixed layer depth (MLD) and only cells with open water are used as a proxy, however the choice of integration and averaging is not straightforward. To highlight the potential issue in using limited area and depth integrations, Fig. 3 shows model results for CanOE-CSIB with integrations to the MLD and for open water cells only (yellow) and for all grid cells (dark blue), and for integrations from surface to bottom depth for open water cells only (cyan) and for all grid cells (pink). With few exceptions, the integration to the bottom overestimates the observed values and shows similar patterns and somewhat higher values than the integration to the MLD only. The effect of only including open water grid cells varies somewhat by region. Generally open water cells capture about 50 to 100% of the total simulated production, suggesting significant under-ice PP in the model. Similar differences also occur in CMOC (not shown), which suggests caution in the interpretation of model-observation comparisons. For this particular case the integration to the MLD for open water grid cells only is most comparable to the Hill et al. (2013) observations and has been used in Figures 2 and 11.

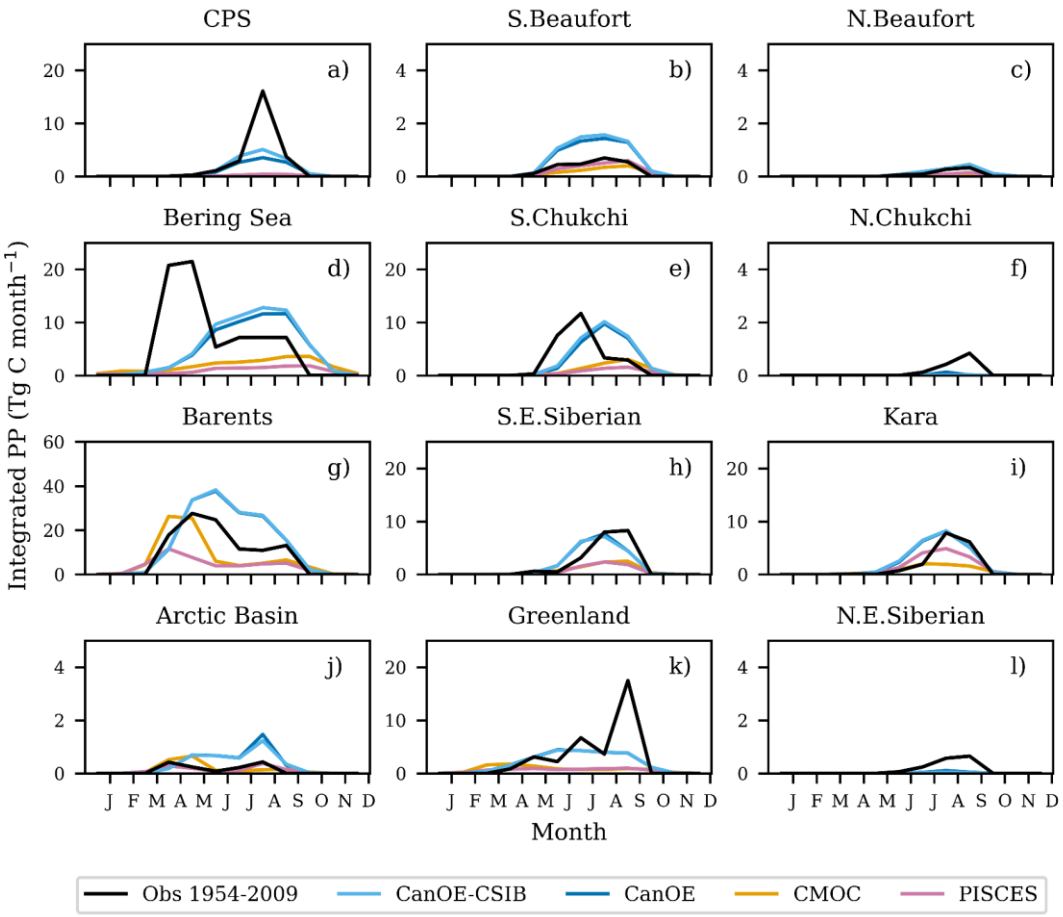

Figure 2: Regionally averaged primary production

Monthly averaged IPP for 1995-2010 (model) and 1954-2009 (Observations). Model results are shown for NAA-CMOC (cyan), NAA-CanOE (green), NAA-CanOE-CSIB (red), and NAA-PISCES (xxx) with integrations over the MLD for open water cells (cells with ice concentrations lower than 50%) (blue) for the Arctic subregions: a) Canadian Polar Shelf (CPS), b) Southern Beaufort Sea, c) Northern Beaufort Sea, d) Bering Sea, e) Southern Chukchi Sea, f) Northern Chukchi Sea, g) Barents Sea, h) Southeast Siberian Sea, i) Kara Sea, j) Arctic Basin, k) Greenland Sea l) Northeast Siberian Sea. (Subregions are indicated in Fig. 1). Observations (black) are from Hill et al. [2013], their Table 4. Note that the observational averages for CPS include the western part of Baffin Bay and the Greenland Sea average includes the Eastern Part of Baffin Bay, while the Baffin Bay is a separate region in the model evaluation.

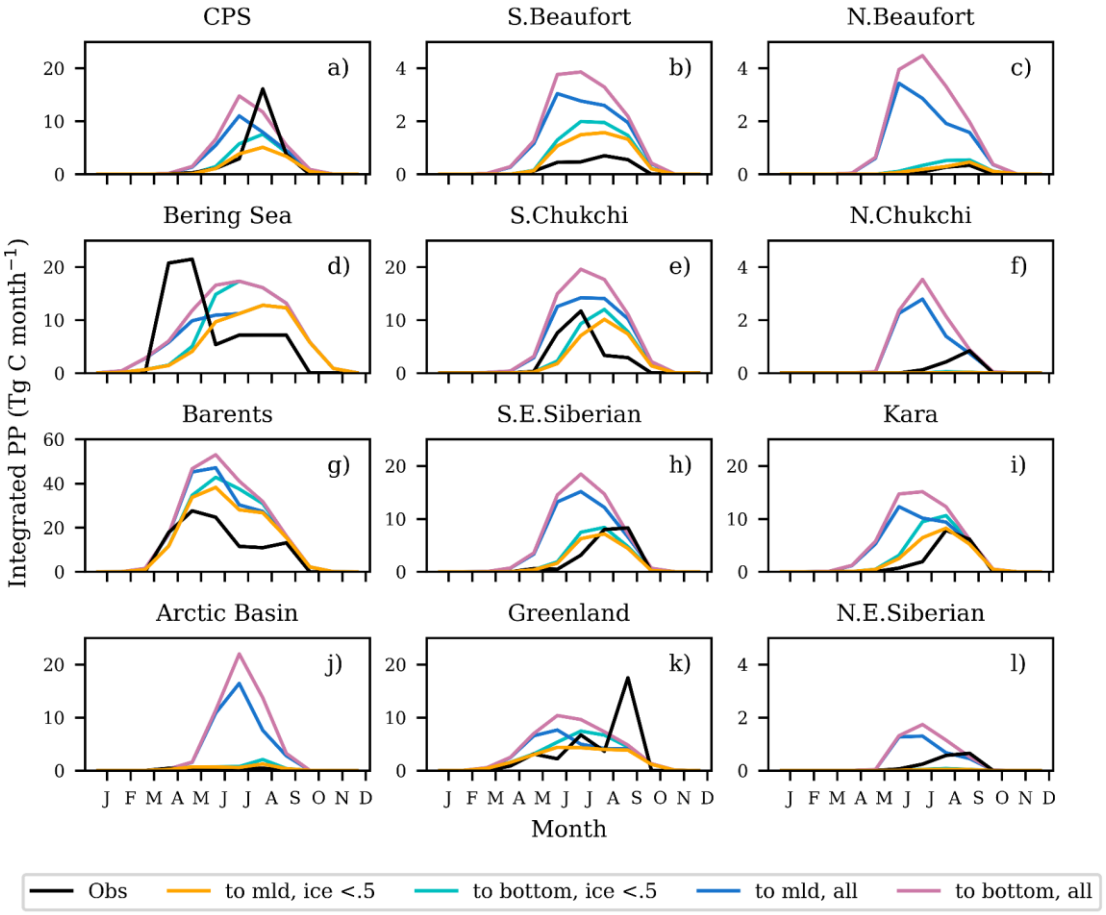

Figure 3: Regionally averaged primary production

a) Monthly averaged IPP for 1995-2010 (model) and 1954-2009 (Observations). Observations are integrated over the euphotic layer. This integration is not computed for the model, hence different integrations are shown to highlight the difficulty in comparing this quantity. Model results are shown for NAA-CanOE with integrations over the MLD and for open water grid cells (grid cells with ice concentrations lower than 50%, red) or for all grid cells (blue),

and for integrations from surface to bottom for open water grid cells (cyan) or for all grid cells (green). PP is shown averaged for the Arctic subregions: a) Canadian Polar Shelf (CPS), b) Southern Beaufort Sea, c) Northern Beaufort Sea, d) Bering Sea, e) Southern Chukchi Sea, f) Northern Chukchi Sea, g) Barents Sea, h) Southeast Siberian Sea, i) Kara Sea, j) Arctic Basin, k) Greenland Sea l) Northeast Siberian Sea. (Subregions are indicated in Fig.1). Observations (black) are from Hill et al. [2013], their Table 4.

3.3. The Subsurface Chlorophyll Maximum (SCM)

SCMs develop every summer after the water column stratifies and surface nutrients are depleted by phytoplankton. Phytoplankton within the SCM cause the nutricline to deepen during the growth season by exhausting the nutrients above. The SCM forms at a depth where light and nutrients remain sufficient to support growth and continuous consumption prevents mixing of nutrients into the upper euphotic zone [Tremblay et al., 2008; Mundy et al., 2009]. Hence, SCMs are frequently located within the pycnocline [e.g., Martin et al., 2010], and are often correlated with the euphotic zone and nutricline depths [Martin et al., 2010; Brown et al., 2015]. Towards the end of the growing season, sea ice starts to form and light availability decreases which eventually causes the SCM community to die off and sink to the ocean floor [Brown et al., 2015]. In some (more southerly) regions enhanced mixing before ice freeze-up in the fall brings up nutrients and initiates a secondary fall bloom [e.g., Ardyna et al. 2014]. The seasonal evolution, maximum depth, Chla concentration and phytoplankton composition varies regionally and is influenced by stratification, nutrients, and source water masses [e.g., Martin et al., 2010; Brown et al., 2015]. The SCM tends to be shallower on the shelves (e.g., 20-30 m in the Chukchi Sea compared to about 60 m or even deeper in the Canada Basin) [Brown et al., 2015].

Figure 4 shows the simulated seasonal cycle of the 1995-2010 climatology for temperature, salinity, and density (same in all biogeochemical models), as well as Chla, NO3 and NH4 for CanOE-CSIB (left), CanOE (row 2), CMOC (row 3) and PISCES (right) for the CPS region. Figures 5 and 6 show similar plots for the Northern Beaufort Sea and Southern Beaufort Sea subregions (regions indicated in Fig. 1). A few distinct patterns emerge: 1) the maximum depth of the SCM is shallower, but with higher concentrations for the CanOE runs than for CMOC and PISCES. 2. CMOC shows a distinct SCM development which is much less pronounced in CanOE and CanOE-CSIB (the Chla maximum moves to slightly deeper depth, but Chla production is retained in the surface ocean). 3. PISCES shows similar SCM depths to CMOC, but lower concentrations. 4. CMOC shows lower NO3 concentrations than the CanOE and PISCES models with depletion in the upper ocean (top ~30 m), NO3 concentrations are slightly higher for CanOE-CSIB than CanOE, and PISCES shows less NO3 drawdown than any of the other models. 5. The CanOE runs develop a pronounced, deep NH4 signal in connection with the phytoplankton bloom which is slightly weaker for CanOE versus CanOE-CSIB. 6. The SCM evolution is clearest in the Northern Beaufort where the maximum Chla is low.

The climatological average masks interannual variations in the onset, depth, and termination of the bloom. Interannually varying Chla and NO3 indicate consistent inter-model differences in the seasonal evolution of Chla and NO3 over the years (not shown).

Additional limitation by Fe in PISCES may be responsible for the development of a SCM, despite a lack of NO3 (and Si, PO4) depletion. In addition, a small but relevant difference in the light attenuation by phytoplankton in PISCES may allow the SCM to extend deeper than in CanOE (see section 3.4.1).

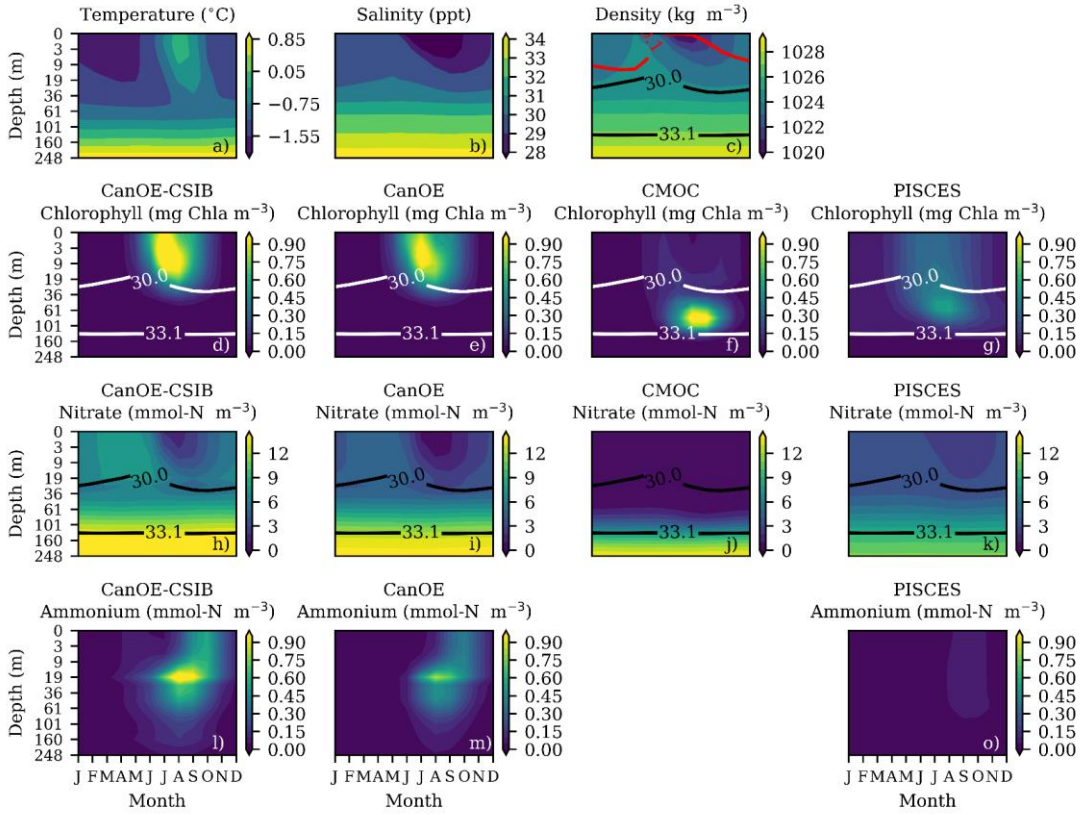

Figure 4: Simulated seasonal cycle for the Canadian Polar Shelf

Simulated climatological mean (1995-2010) seasonal cycle by depth, averaged for the Canadian Polar Shelf subregion: a) temperature [m], b) salinity [ppt], c) density [kg m^{-3}], Chla [mg-Chla m^{-3}] for d) CanOE-CSIB, e) CanOE, f) CMOC, g) PISCES, nitrate NO3 [mmol-N-a m^{-3}] for h) CanOE-CSIB, i) CanOE, j) CMOC, k) PISCES and ammonium NH4 [mmol-N-a m^{-3}] for l) CanOE-CSIB and m) CanOE and o) PISCES. (CMOC does not simulate NH4 concentrations). For reference, white and black lines indicate salinities of 33.1 and 30.0. The red line in c) indicates the depth where density changes by 1 kg/m3 from surface (<10m) as a proxy for the mixed layer.

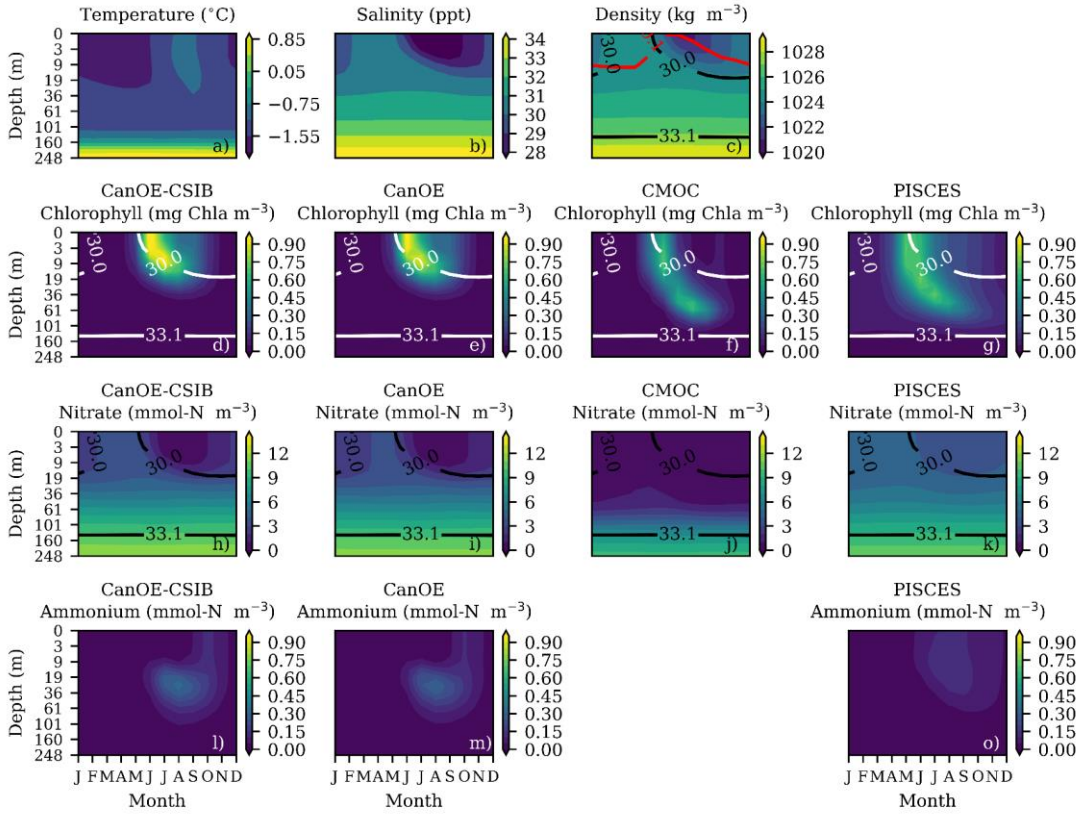

Figure 5: Simulated seasonal cycle for the Northern Beaufort Sea

As Fig. 4 for the Northern Beaufort Sea subregion

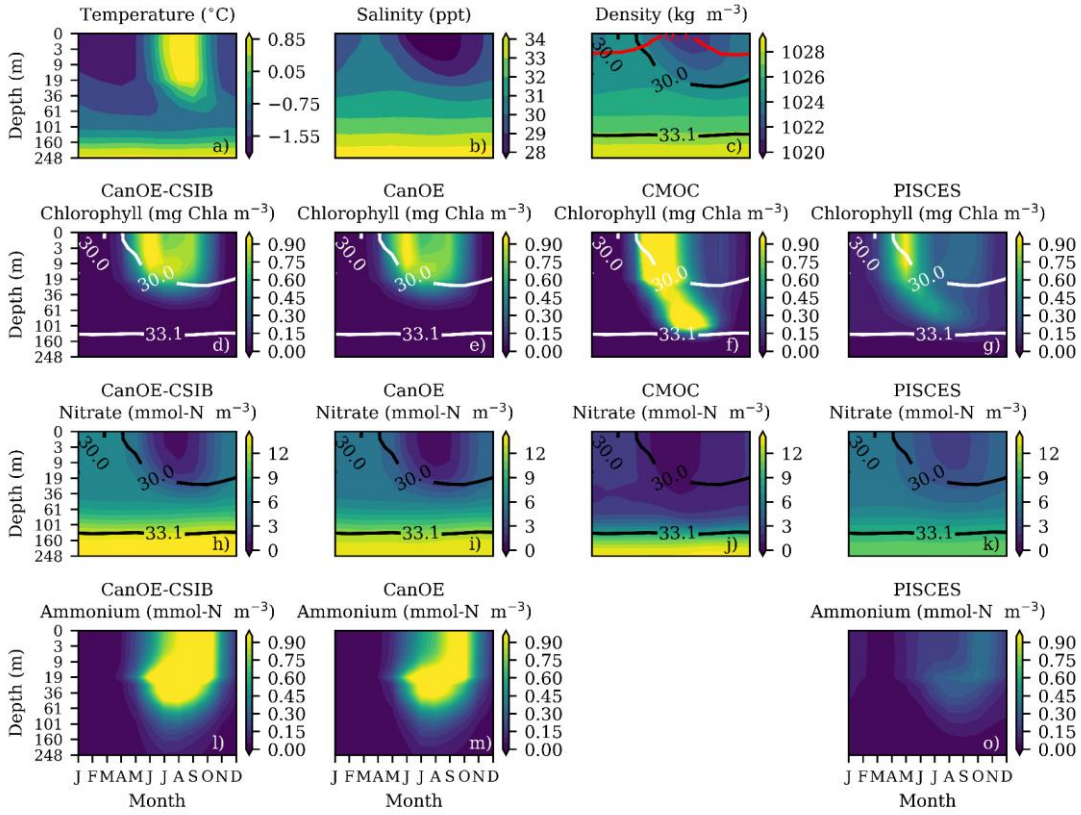

Figure 6: Simulated seasonal cycle for the Southern Beaufort Sea

As Fig. 4 for the Southern Beaufort Sea subregion

3.4. Canada's 3 Oceans (C3O) transect

Differences in the representation of the SCM also emerge along the Canada's 3 Oceans (C3O) transect line, following the ship track from the Pacific through the Canadian Arctic into the Atlantic [Carmack et al., 2010]. Fig. 7 indicates the Arctic portion of the C3O transect in white on the background of simulated sea surface temperature, Chla and sea-ice thickness for CanOE-CSIB (note that temperature and sea-ice thickness are the same for all biogeochemical models). Fig. 7 shows highest Chla concentrations near the Beaufort Sea coast where the ice has retreated, and the waters have warmed. There is little surface Chla shown along the transect in the Beaufort Sea and in Baffin Bay. The observed Chla during July and August 2007 indicates production in the surface ocean for the Bering Sea Shelf (H to I) with a developing SCM in the Beaufort Sea (I to J), a developed SCM in the Beaufort Sea (J to M) and most of the Canadian Polar Shelf (N to T) and surface production in the Amundsen Gulf (M to N) and Baffin Bay/Davis Strait (T to W) (Fig. 8) (note that locations K and L are excursions into the central Beaufort Sea, which are not included in the model transect). The observed SCM occurs to depths up to 100 m (note that Chla is given on a log scale in Fig. 8). Figure 9 shows the C3O transect (subset stations H to W/OSB) for model runs with CanOE-CSIB, CanOE, CMOC, and PISCES for August 2007 (June 2007 is shown in supplementary figure S1). Following predominantly near-surface production in June, the model results indicate SCM development in July (not shown) and August. CMOC reproduces the observed extent of SCMs and Chla production at depths similar to the observations (60-100 m) depth.

For CanOE-CSIB and CanOE, simulated Chla is higher in the near surface and the SCM is generally shallower (20-40m). PISCES reproduces a deeper SCM but shows much lower concentrations. Note that the C3O cruise travelled from the Pacific to the Atlantic within one month in July/August 2007, and the observations may represent some potentially short-lived events. In contrast, the model figures show monthly averages that do not adequately represent short-lived high surface production events or the brief appearance of a weak SCM as shown in the observations.

The CanOE models, particularly CanOE-CSIB, do not reproduce a SCM over the shallow shelves of the CPS (between N and O). Nutrient concentrations are shown for NO3 for August (Fig. 10) and for June (Fig. S2), and NH4 and Fe (PISCES only) concentrations in August (Figures S3 and S4) and June (Figures S5 and S6). Both CanOE versions and CMOC reach near NO3 depletion in the water mass above the SCM (depletion ranges deeper for CMOC). An exception is the center of the CPS region, which is dominated by narrow channels and shallow shelves, where particularly CanOE-CSIB retains NO3 in the upper water column with somewhat lower values for CanOE and depletion in CMOC (Fig. 10 and Fig. S2, Appendix 1). PISCES on the other hand shows NO3 throughout most of the transect, suggesting that NO3 is not fully utilized. Both CanOE models show an accumulation of NH4 extending into the upper water column from the bottom, building up in June (Fig. S5), with consequent depletion (above the SCM) into August (Fig. S6). This is related to the remineralization of sinking detritus particularly in CanOE-CSIB where fast sinking ice-algal detritus is produced earlier in the season before the pelagic bloom. Nitrification only occurs in the dark and NH4 can accumulate in shallower regions over the summer. This NH4 accumulation is responsible for the limitation of NO3 uptake (see section also 4.1.2). As for NO3, PISCES retains NH4 in the upper water column, suggesting inability to fully access N-based nutrients.

Reviewing the additional nutrients simulated in PISCES, both PO4 and Si show similar patterns of partial drawdown, however, Fe shows depletion in the upper water column, suggesting that within PISCES the system becomes iron limited (supplementary figures S4, S6). Iron has not generally been considered a limiting nutrient in the Arctic; hence the Fe limitation parameterisation has been removed from the CanOE experiment and CMOC does not have Fe limitation at these locations. However, recent observations indicate potential Fe-limitation for under-ice blooms in Arctic waters [Rijkenberg et al. 2018], suggesting revisiting the inclusion of Fe limitation in Arctic ocean ecosystem models.

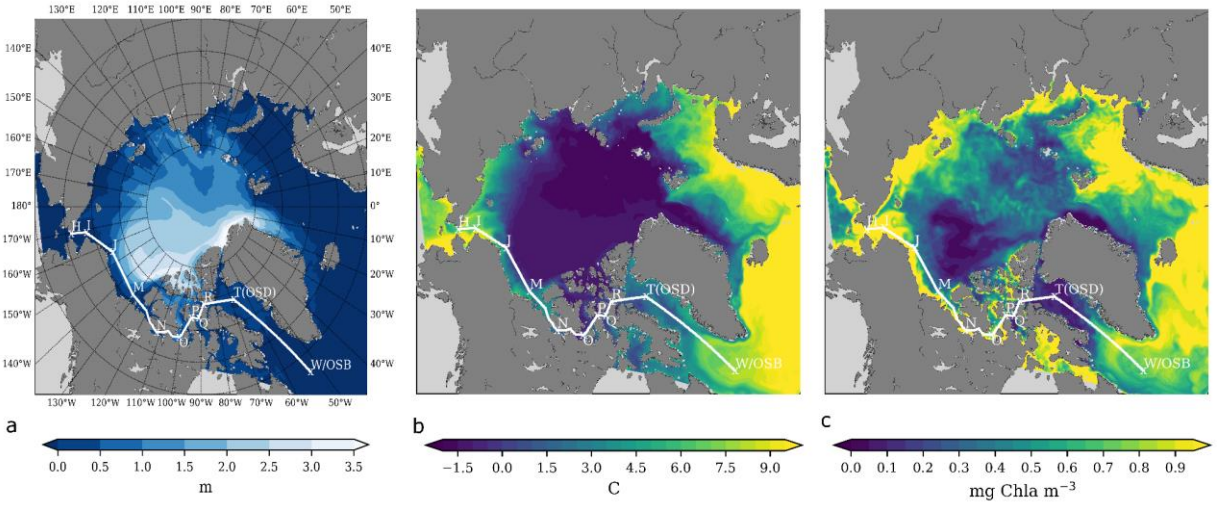

Figure 7: Pan-Arctic model simulations and transect location

a) Simulated ice thickness averaged for July, August, September (JAS) in 2007 , b) Simulated surface temperature [^{o}C], and c) simulated Chla [mg-Chla m^{-3}]. White line indicates the Canadian 3 Oceans (C3O) cruise transect. Model simulations are from NAA-CanOE-CSIB, however physical variables (a,c) are identical for all biogeochemical modules.

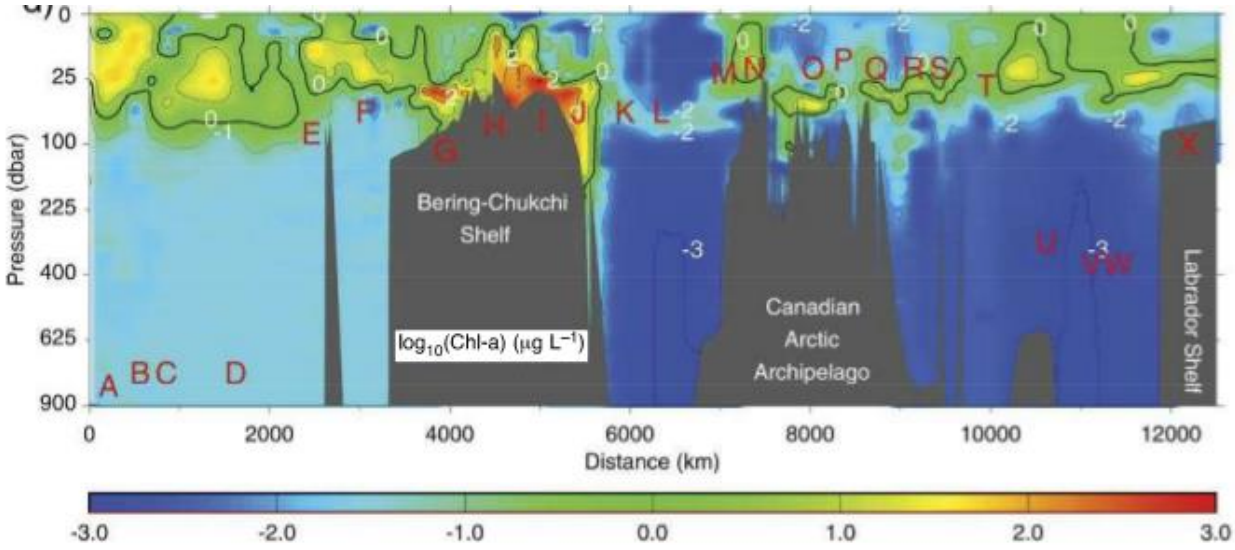

Figure 8: Observed Chla along the C3O transect in July/August 2007

Observed Chla (log10 (Chla) [µg L^{-1}]) during the C3O cruise in July/August 2007 (transect from the Bering Strait, I, to W indicated in Fig. 7). From Carmack et al. (2010).

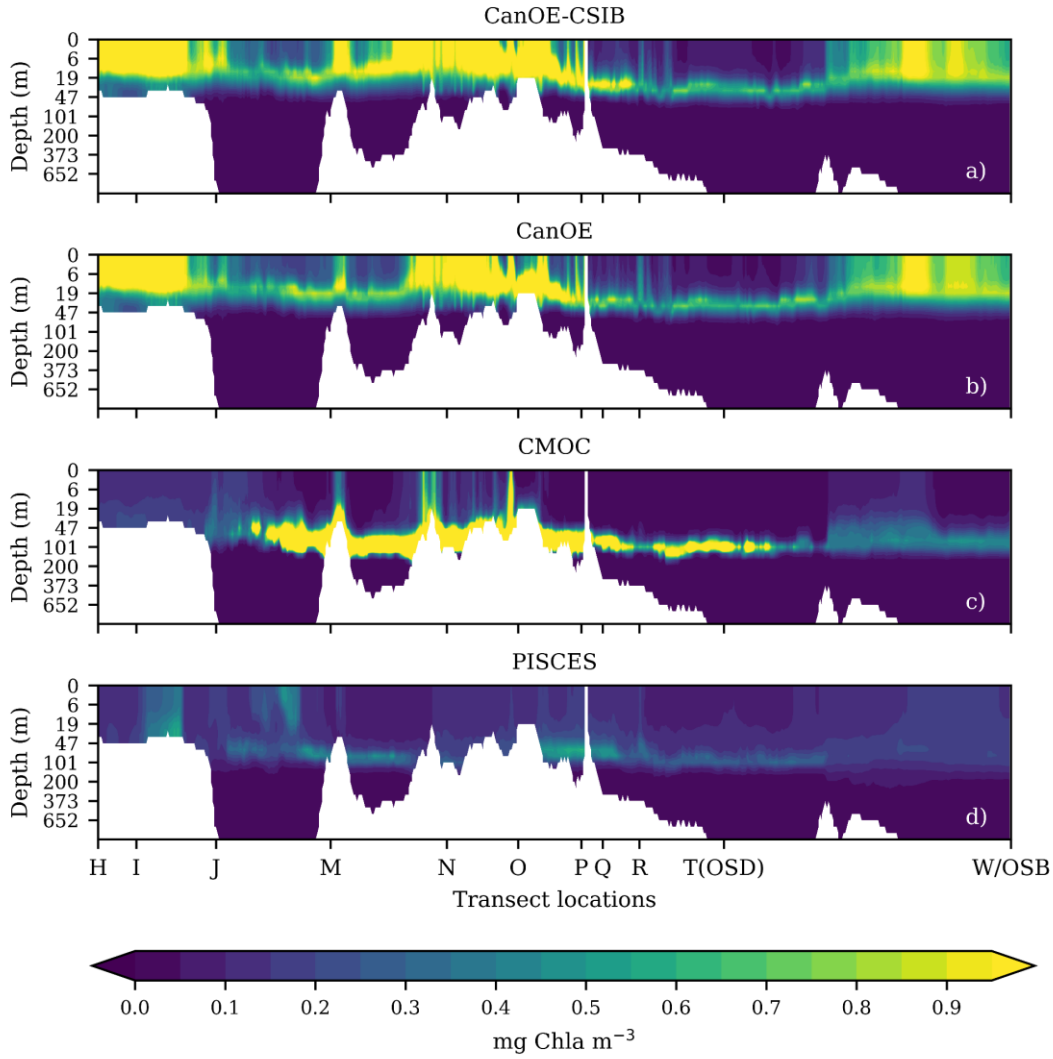

Figure 9: Simulated Chla along the C3O transect in August 2007

Simulated Chla [mg-Chla m^{-3}] for August along the C3O transect indicated in Fig. 7 for a) NAA-CanOE-CSIB, b) NAA-CanOE, c) NAA-CMOC, d) NAA-PISCES

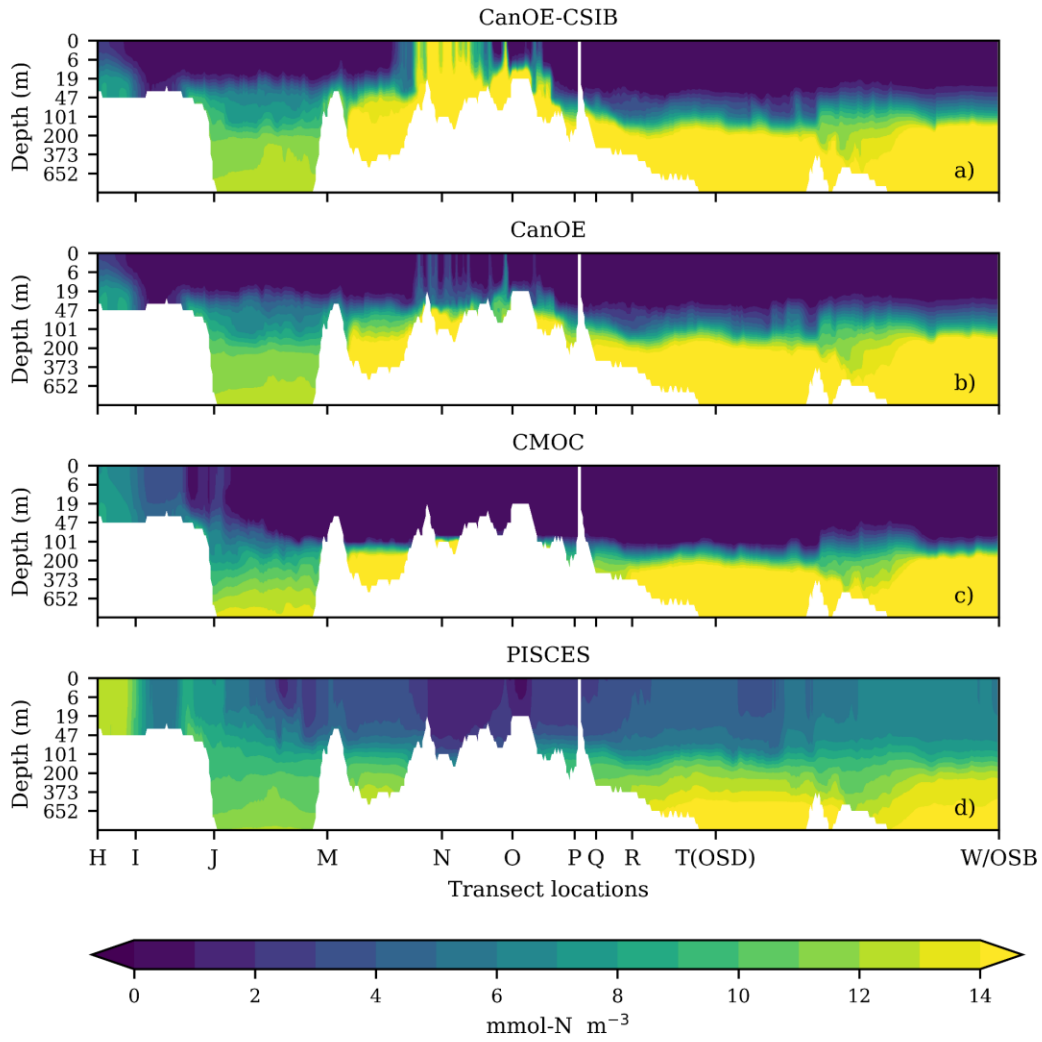

Figure 10: Simulated NO3 along the C3O transect in August 2007

Simulated NO3 [mM-N m^{-3}] for August along the C3O transect indicated in Fig. 7 for a) NAA-CanOE-CSIB, b) NAA-CanOE, c) NAA-CMOC, d) PISCES.

3.4.1. Water column light attenuation

Light is attenuated in the water column and is absorbed by phytoplankton Chla, limiting light availability to the layers below. This has been identified as a key cause for differences among simulations of primary production and Chla. The standard NEMO-PISCES light attenuation in

each model layer depends on the spectral absorption by water of three distinct bands of light (red, green, and blue) [Morel and Maritorena, 2001] and three different Chla-concentration dependent absorption coefficients for each of the two phytoplankton and the detritus groups. PISCES absorption coefficients are based on the data synthesis by Bricaud et al (1995) who named the pigmentation composition in phytoplankton and a size effect due to pigments packaging which weights differently on the contributions of the three wavelength bands as reasoning for the different absorption coefficients, but highlight that the results are based on data from limited regions and times. (Observations of diffuse attenuation coefficients in the water column of the Canada Basin from Antoine et al , 2013, with Chla-depended coefficients from Aumont et al, 2015, are shown in supplementary figure S7).
CanOE uses the same spectral (3-band) attenuation as PISCES, but Chla-dependent attenuation depends only on total Chla. CMOC light attenuation uses a simpler scheme with a single (spectrally averaged) band, with constant water attenuation plus a linear Chla concentration dependence [Zahariev et al., 2008] (see Table S1, Appendix 2). To evaluate the impact on the Chla signal, a light attenuation experiment has been carried out in the 3-D model. The simpler CMOC and more complex PISCES schemes have been implemented in CanOE-CSIB in lieu of the standard CanOE parameterisation and run for the year 2007. Figure 11 shows a comparison of the simulated seasonal cycle of Chla in 2007 for four subregions (as shown in Fig.1), the Canadian Polar Shelf (a-c), Northern Beaufort Sea (d-f), Southern Beaufort Sea (g-i) and the Baffin Bay (j-l) subregion with original CanOE attenuation (left), CMOC-style attenuation (middle), and PISCES-style attenuation (right).The seasonal Chla pattern is very similar for the three parameterizations for each region. However, the SCM is consistently deeper and sharper for the CMOC-style attenuation and slightly deeper for the PISCES-style attenuation than for the CanOE attenuation. The impact on the SCM depth is also seen in the modelled C3O transect: the standard CanOE-CSIB run shows highest Chla concentrations at depths of about 20, 50 and 25 m for the Beaufort Sea, Amundsen Gulf and Baffin Bay (Fig. 9a), respectively. Applying the CMOC (PISCES) parameterizations leads to depths of 50 (30), 75 (70) and 50 (35-40) m (not shown).

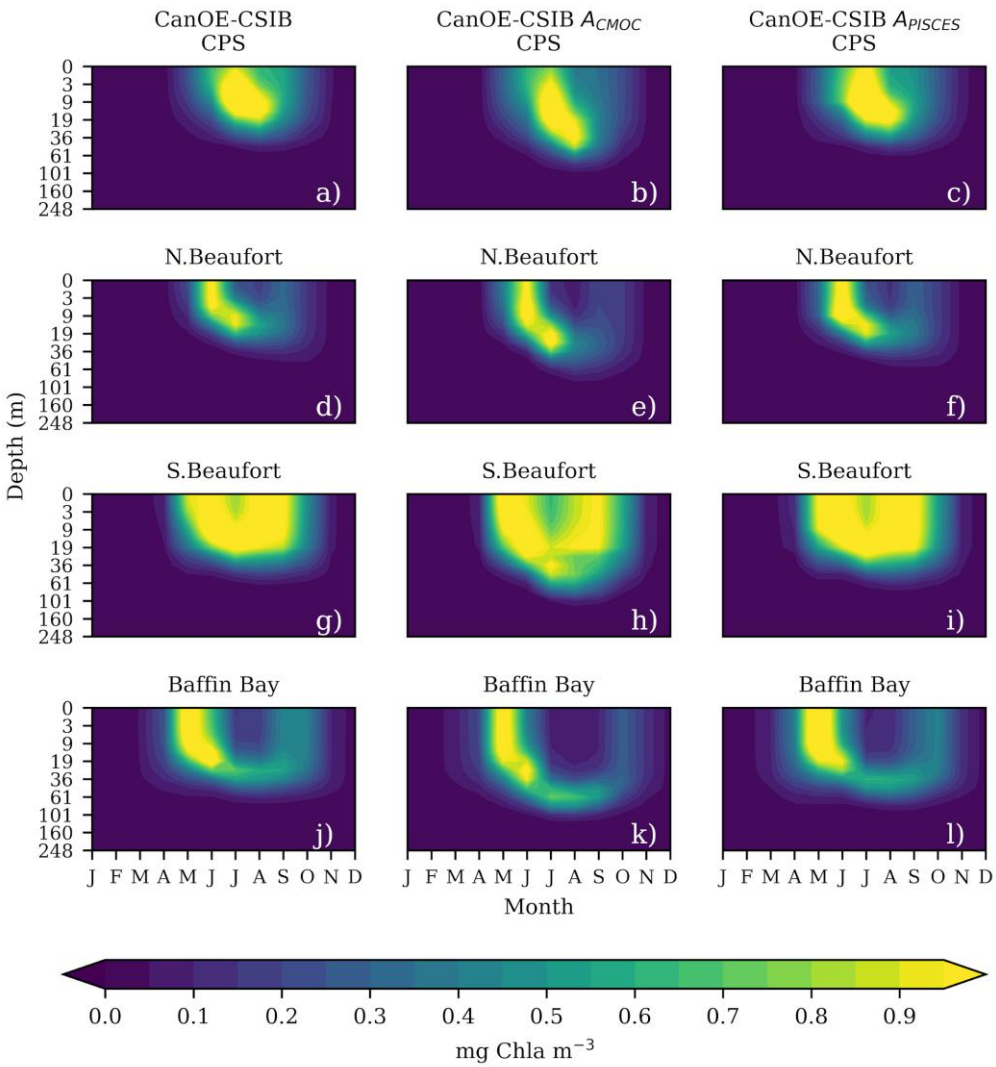

Figure 11. Simulated seasonal cycle of Chla with different light parameterizations

Simulated seasonal cycle of Chla [mg-Chla m^{-3}] in 2007 for the Canadian Polar Shelf, Northern Beaufort Sea, Southern Beaufort Sea, and Baffin Bay subregions for NAA-CanOE-CSIB with different light attenuation parameterizations: CanOE attenuation (A_{CanOE}, left), light attenuation as in NAA-CMOC (A_{CMOC}, middle), attenuation as in PISCES (A_{PISCES}, right), see text for details.

3.5. Trends in integrated primary production and phytoplankton concentration

Fig. 12 compares CanOE-CSIB results for the various decades and averaging periods and suggests that most regions show small changes in PP over time, with highest rates occurring in different decades in different regions. Some of the patterns in the long-term observational average could be biased towards periods with more observations and individual peaks may be biased by individual years with very low ice cover exposing open water regions with high PP. However, in general the seasonal pattern seems to remain consistent across decades and

characteristic for each region. Given the differences in biogeochemical models it is important to understand how these differences manifest in mean primary production and long-term trends. Figure 13 shows the simulated trends for the various regions for CanOE-CSIB with respective trends for CMOC and PISCES in the supplementary figures (S8, S9). For CanOE-CSIB and PISCES, most of the PP is within the top 20m, so adding lower layers into the integration changes the total only slightly, while in CMOC the 50 and 100m integrations capture additional production with similar interannual variability. Comparing total PP (blue line) among the models shows very similar trends, interannual variability and regional differences. The magnitude of the integrated PP differs by less than 15% between those models. In addition to the lower overall PP, the PISCES model shows much lower interannual variability. This is likely due to the limited depletion of available macronutrients which suppresses the impact of interannual variations in light or nutrients. The long-term trends show an increase in all regions, except for a slight decrease in the Greenland Sea and fairly constant values in the Arctic Basin. PISCES trends are less obvious. We can compare the model results to regionally averaged observation-based primary production trends summarized in Frey et al. [2018]. While the trends are not directly comparable due to the temporal difference and regional averaging, the observations show similar patterns and similarly high interannual variability as in the CanOE and CMOC models.
Statistics for simulated mean and trends (from 1980 to 2015) in IPP integrated over the top 100 m for spring (April, May, June, AMJ) and summer (July, August, September, JAS) in the regions indicated in Fig. 1 provided in Supplementary Table S2 (Note that units are in Tg-C y^{-1}, to calculate total production over one season the values need to be divided by four). Table S3 shows respective integrations for phytoplankton concentration (Appendix 3). With few exceptions CanOE-CSIB shows higher values in the central and North American Arctic and CMOC shows higher values in the European and Siberian Arctic for spring and summer. PISCES shows mostly lower values. All models are consistent in the representation of unproductive regions versus highly productive regions. PISCES shows similar magnitudes for the low production region, but does not simulate very high PP, particularly in the Barents Sea. Hence PISCES shows a pan-Arctic mean of less than half of what is simulated in CanOE-CSIB and CMOC.
Integrated over the whole Arctic region (north of 66.5^{o}N), mean PP for CanOE-CSIB (CMOC) is 965 (1119) Tg-C y^{-1} in spring and 1093 (1190) Tg-C y^{-1} in summer compared to 384 Tg-C y^{-1} (spring) and 446 Tg-C y^{-1} (summer) for PISCES. It is possible that the Fe limitation is responsible for a cap on PP in PISCES. PISCES PP is much lower than observational estimates or other models, so the application of Fe limitation in Arctic models may require additional evaluations and testing. Except for the Barents Sea where sea ice retreats early, the models show highest production in summer. The trends are almost exclusively positive (or near zero), except for Baffin Bay (spring and summer trends are negative, Table S2, S3). Baffin Bay is not included in Fig. 13, but the annual trends are also negative. CMOC also shows a slight negative trend in summer for the Kara and Barents regions. With a few exceptions, the trends are significant at the 95% level ($P < 0.05$). The same regional patterns and trend directions are also visible in the phytoplankton concentrations (Table S3).
Production is low to negligible in fall (32/58/25 Tg-C y^{-1} for CanOE-CSIB/CMOC/PISCES, respectively) and winter (12/87/42 Tg-C y^{-1}).

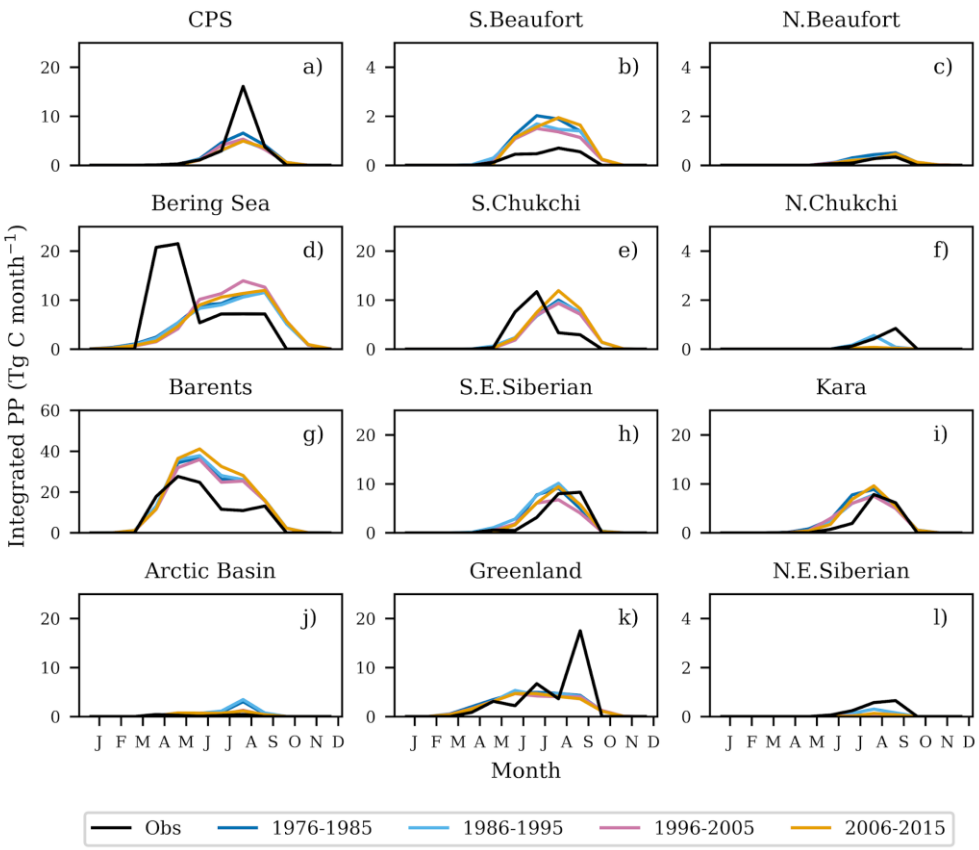

Figure 12: Decadal change in primary production
Monthly averaged IPP for CanOE-CSIB and observations (1954-2009).
Model results are averaged over 1976-1985 (dark blue), 1986-1995 (cyan), 1996-2005 (pink), 2006-2015 (yellow). Model integrations are over the MLD for open water cells (grid cells with ice concentrations lower than 50%) for the Arctic subregions: a) Canadian Polar Shelf (CPS), b) Southern Beaufort Sea, c) Northern Beaufort Sea, d) Bering Sea, e) Southern Chukchi Sea, f) Northern Chukchi Sea, g) Barents Sea, h) Southeast Siberian Sea, i) Kara Sea, j) Arctic Basin, k) Greenland Sea l) Northeast Siberian Sea. (Subregions are indicated in Fig.1). Observations (black) are from Hill et al. [2013], their Table 4.

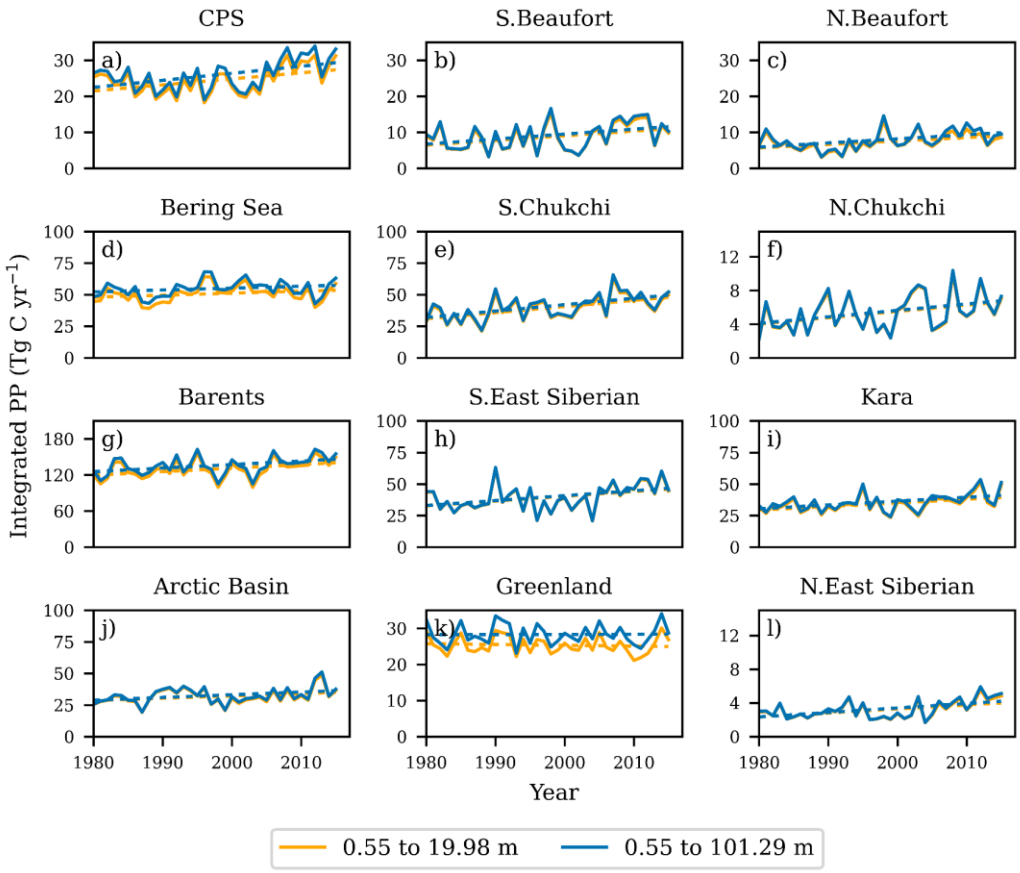

Figure 13. Simulated trends in primary production for CanOE-CSIB

Simulated PP [Tg-C y^{-1}] for 1995-2010, integrated over the upper 20 m (yellow) and 100 m (blue) (Note, for CanOE-CSIB, the 50 m integration is essentially the same as the 100 m integration and hence not shown). Model results are shown for CanOE-CSIB for the Arctic subregions: a) Canadian Polar Shelf (CPS), b) Southern Beaufort Sea, c) Northern Beaufort Sea, d) Bering Sea, e) Southern Chukchi Sea, f) Northern Chukchi Sea, g) Barents Sea, h) Southeast Siberian Sea, i) Kara Sea, j) Arctic Basin, k) Greenland Sea l) Northeast Siberian Sea. (Subregions are indicated in Fig.1).

4. 1D-MODEL SENSITIVITY STUDIES

Model differences usually originate in differences in responses to environmental changes due to limited understanding of physical and biological processes. This leads to differences in modelling approaches and parameterizations. In multi-model output analyses, including the analysis of future projections, these differences contribute to the model response uncertainty [Kirtman et al., 2013] and the spread among different models is used as a measure of the range of model response uncertainty. Here we assess differences in the evolution of the SCM due to sinking, growth and mortality rates through parameter sensitivity studies within the 1-D GOTM model [Umlauf and Burchard, 2005, ttps://gotm.net/about]. The model set-up follows Mortenson et al. [2017]. Within the first 100 m of the water column, summer chlorophyll observations for

Resolute in 2010 approach a maximum of 10 mg-Chla m^{-3} [see Mortenson et al., 2017, their Fig. 5b]. Note that the CanOE run simulates maximum Chla values of about 2.5 mg-Chla m^{-3} only, compared to 8 mg-Chla m^{-3} for the original GOTM run [Mortenson et al., 2017].

4.1. Growth, mortality and sinking rates

Sensitivity to growth, mortality and sinking rates was assessed by changing the rate parameters as indicated in Table 1. Higher phytoplankton growth rates allow faster growth, but also faster depletion of nutrients, which may accelerate the development of a SCM but also increase the biomass at a given time. Increased mortality rates accelerate the transfer from the live phytoplankton pools to the detrital pools which reduces the strength of the bloom and associated Chla signal. This also reduces the uptake of nutrients and may weaken the development of a SCM. As detrital material then sinks towards the bottom, higher mortality rates also lead to faster removal of material from the surface. This can be further accelerated by increasing the detrital sinking rates.
Figure 14 shows GOTM-CanOE individual and combined responses to an increase in the reference light saturated growth rate P^C_{ref} (to the right) and increasing detrital sinking rate. In CanOE the light-limited growth rate is given as

$P^C_{phot} = P^C_{max}\ (1 - e\ \hat{}\{-\alpha_{chl}\ E\ \Theta_c\}/\{P^C_{max}\});$ with

$P^C_{max} = P^C_{ref}\ T_f\ min\{(Q^N - Q^N_{min})/(Q^N_{max} - Q^N_{min})\}$ (1)

where P^C_{max} is the maximal carbon-based growth rate and P^C_{ref} is the light saturated growth rate at the reference temperature T_{ref} under nutrient-replete conditions ($Q = Q_{max}$). Q is the nutrient N cell quota and Q_{min} and Q_{max} its minimum and maximum values; α_{chl} is the initial slope of the photosynthesis-irradiance curve (PI), E is the irradiance and Θ_C is the chlorophyll-to-carbon ratio. A full record of the equations in CanOE is given in Christian et al [2022]. (Note that the version of CanOE used here does not include iron limitation). The applied increase of P^C_{ref} has only a slight effect on the evolution of the SCM (SCM descends faster) but increases the Chla concentration in the bloom. A similar effect to increasing the growth rate is seen when the mortality rate is decreased (Supplementary Fig. S10). CanOE has a linear and a quadratic mortality term with, under most conditions, a higher contribution to the total mortality from the linear term (not shown), hence the SCM response is stronger for a decrease in linear mortality. The effect of reducing the Chla signal dominates and runs with increased mortality show a clearly reduced Chla signal and a weaker and shallower SCM (Appendix 1, supplementary figure S10). The initial PI-curve slope α_{chl} also affects growth with a larger α_{chl} allowing the phytoplankton to grow faster under low light. Hence, increasing α_{chl} increases the Chla magnitude, but does not affect the evolution of the SCM (Appendix 1, supplementary figure S11).
Detrital sinking affects the location for remineralization. If the sinking rate is small, detritus remineralization occurs closer to the surface, allowing for nutrient replenishment and continued growth. Fast sinking detritus strips nutrients out of the surface layers more efficiently. Figure 14 shows that an increased sinking rate affects the evolution of the SCM by deepening of the upper depth limit of production, and leads to a more pronounced SCM. The sinking rate does not affect the Chla concentration in the SCM.
To compare rates chosen here to those used in the 3D models, the sinking rates for CanOE, CMOC and PISCES are indicated in Table S1 (Appendix 2). Note that sinking rates in the range of 6-10 m d^{-1} are on the lower range for large as well as aggregated particles, while 1-3 m d^{-1} is more appropriate for small detritus. The availability of multiple detritus pools within a biogeochemical model accounts for these differences and affects the nutrient remineralization

depth. For example, if the pelagic phytoplankton community is dominated by small phytoplankton, contributions to the small, slow sinking detrital pool is larger and remineralization can stay closer to the surface. Ice algae tend to aggregate and contribute to the large, fast sinking detritus pool, which supports a system that is more efficient in stripping nutrients from the surface ocean. This can have a large effect on the development of the SCM [e.g., Mortenson et al., 2017], which can be exacerbated if the dissolved N pool is separated into NO3 and NH4 (see section 4.1.2). (Note that excluding temperature effects on biogeochemical processes enhances the sensitivity to parameter changes). In the 1-D model sensitivity test, changing the sinking and growth parameters can achieve some improvement (i.e., deepening and intensification of the SCM), but the adjustments in CanOE are insufficient to allow SCM developments at the observed depths.

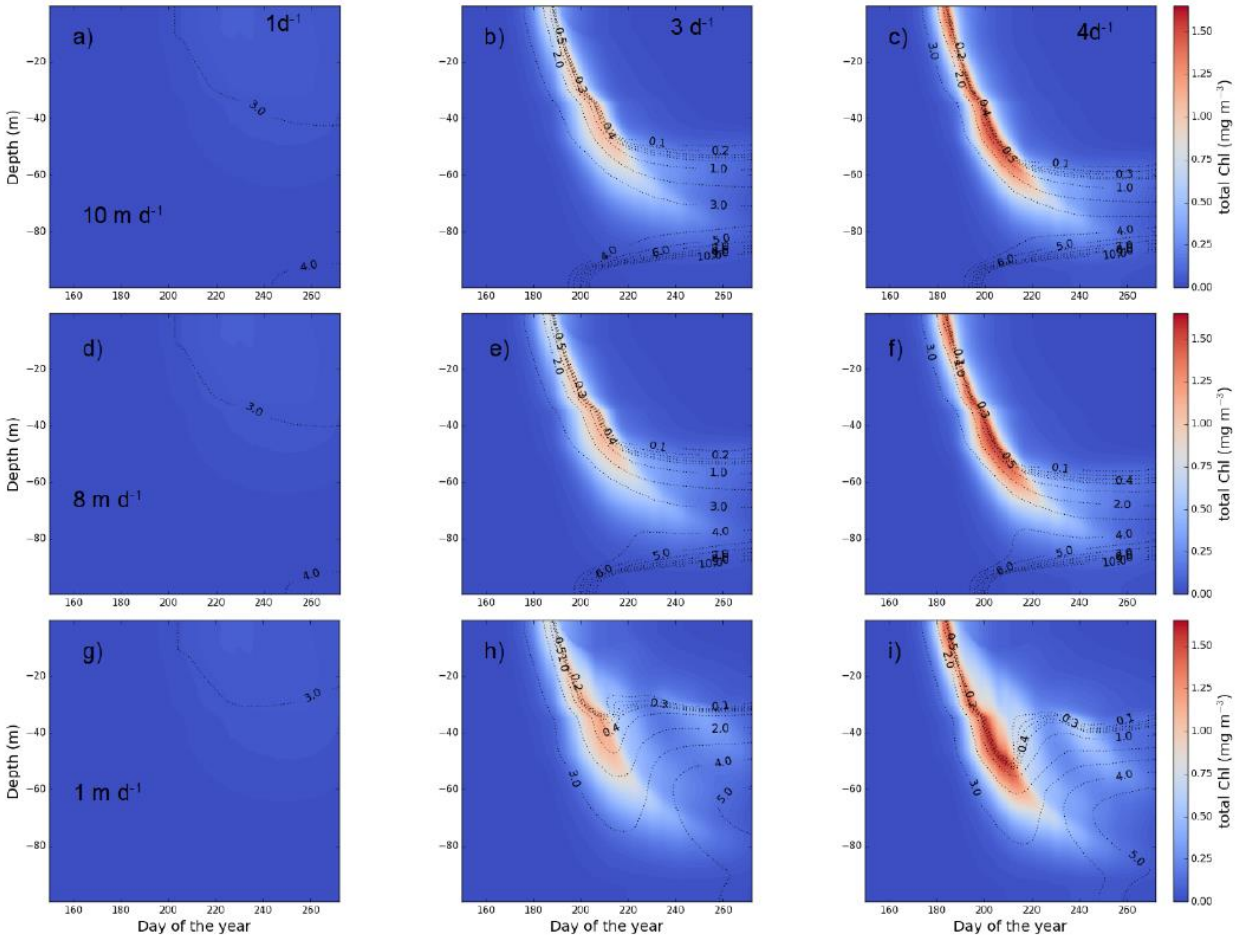

Figure 14
Simulated Chla [mg-Chla m^{-3}] for sensitivity studies with GOTM-CanOE at the Resolute Bay location on the Canadian Polar Shelf (74ºN, 95ºW) in spring to summer 2010. Results show individual and combined responses to an increase in light saturated growth rate ($1d^{-1}$, $3d^{-1}$, $4d^{-1}$ from left to right) and decreasing sinking rate (10 md^{-1}, 8 md^{-1}, 1 md^{-1} from bottom to top). Black contour lines indicate nutrients (NO_3 in 1 µM increments).

4.2. Nitrogen dependence

One of the key differences among CanOE, CMOC and PISCES is the nitrogen limitation. CMOC has a DIN pool, but no explicit pool for NO3 or NH4. In both CanOE and PISCES, NO3 and NH4 are explicitly represented. In addition, in the nutrient uptake parameterization in CanOE, NH4 is preferred over NO3, i.e. nutrient saturation is more quickly reached for NH4 (0.05 µM)

than NO3 (0.1 µM for small, and 1 µM for large phytoplankton) and phytoplankton NO3 uptake will be strongly reduced if there is NH4 at concentration levels at least close to the NH4 half-saturation constant (inhibition of NO3 uptake by NH4), i.e. NO3 uptake occurs only as long as NH4 is below 0.05 µM. Parameterizations of nitrogen limitations in ecosystem modelling have been reviewed in Hood and Christian [2008]. The parametrization suggested by Vallina and Le Quéré [2008] (their Eq. 9) and a very similar parametrization based on Parker [1993] [Tian, 2006, their eq.22] have been highlighted as being more adequate than other functions with respect to this inhibition effect, and are used in CanOE. However, as indicated above (3.4) on shallow polar shelves with limited advective flow and no nitrification due to polar light, NH4 can potentially accumulate to very high values and prevent drawdown of NO3.
In the 1-D model we compared CMOC and CanOE in GOTM (not shown). For CMOC, the phytoplankton bloom deepens until it stabilizes in July and August close to the nutricline (determined by the sole DIN pool, around the 1 µM isopleth). For CanOE, Chla decreases near the surface and does not show a continuous deepening. The Chla vertical distribution is strongly coupled to the NH4 availability. A test run with a 10-fold increase in initial DIN shows only a weak response in CanOE, with a bloom similar to the low DIN case, while it leads to a deeper bloom in CMOC, following the nutricline (not shown). This suggests that in CanOE the NO3 uptake inhibition by NH4 might prevent the adequate development of a SCM at least in some regions.

4.3. The chlorophyll to carbon ratio

Chla production is linked to phytoplankton cell growth via either constant or variable ratios of Chla:C or Chla:N (Θ_C, Θ_N) (a maximum ratio under low light, reflects the assumption that phytoplankton maximize their photosynthetic efficiency, e.g. Kana and Glibert, 1987; Geider et al., 1996). Different parameterizations or values of Θ_C or Θ_N result in different modelled Chla concentrations and representation of the SCM [see also Steiner et al. 2015]. Both CMOC and CanOE use variable Θ. In CMOC, Chla changes are calculated as the product of the phytoplankton source and sink terms and Θ_N, where Θ_N is relaxed to a balanced-growth Θ_N (Geider et al, 1997; Zahariev et al, 2007; 2008). By comparison, CanOE has two phytoplankton functional groups, and each group has four state variables: C, N, Fe and Chla. Photosynthesis is decoupled from cell production and the photosynthetic rate is a function of the cell's internal N and Fe quotas. Chlorophyll synthesis is a function of N uptake and increases at low irradiance (Christian et al. 2022).

A strong contrast between the simulated Θ in CanOE and CMOC is seen during the winter pre-bloom period (both for 1-D and 3D simulations) (e.g. supplementary figure S12). In the 1-D sensitivity study, we tested the impact of increasing and decreasing the initial Chla from a standard value of 2×10^{-3} mg-Chla m^{-3} to 2×10^{-2} and 2×10^{-4} mg-Chla m^{-3} and the standard value of phytoplankton C from 10^{-2}µM-C to 10^{-1} and 10^{-3} µM-C. (The standard values were based on winter Chla data from the literature, e.g. Berge et al., 2015). These changes had only a minor effect on the bloom chlorophyll and Θ. The higher initial carbon slightly reduces the Chla maximum value while higher initial Chla slightly increases the Chla concentration before the bloom and increases the 90-100 m Chla. Hence, Θ is mainly affected before the bloom and below 70-80 m during summer.
In CanOE, the Chla and C production is low due to the high irradiance. CMOC, on the other hand, shows high Θ during the bloom in spring and summer with maxima of Θ_{max} =0.03. This is due to the forced relaxation to a balanced Θ in the CMOC parameterization which leads to a Θ maximum at low irradiance [Zahariev et al., 2007; Geider et al., 1997].

Summary

Despite improvements in our understanding of biogeochemical processes and increasingly complex model parameterizations, limits to accurate simulation of Arctic biogeochemistry remain across various models. Limited availability of spatially and temporally resolved observations e.g., of primary production and chlorophyll, still impedes our ability to evaluate marine productivity simulated in models. However, we can advance our understanding through model intercomparisons. To evaluate the impact of biogeochemical model parameterizations, three biogeochemical models have been compared within the same 3D physical model framework, and additional sensitivity studies have been performed within a 1-D model framework. Compared to available observations, the CanOE-CSIB model reproduces observed PP in most regions of the Arctic but tends to overestimate it in regions with low nutrient conditions, and does a poor job if simulating the slow evolution of the subsurface chlorophyll maximum (SCM) across the Beaufort Sea and CPS. The 3-D model intercomparison highlights that in contrast to CanOE-CSIB, the much simpler CMOC model simulates a more realistic temporal evolution as well as depth of the SCM. CanOE without a sea-ice algae component shows slight differences in the seasonal evolution and near surface concentrations, but the seasonal evolution of the SCM is similar to CanOE-CSIB. The PISCES model shows only partial drawdown of NO3, NH4, PO4 and Si, and underestimates total primary production. This is related to Fe limitation, which is not included in the other two models.

We conclude that: 1) the models exhibit marked differences in the seasonal evolution of phytoplankton concentrations affecting vertical distribution of chlorophyll, specifically the seasonal evolution of the SCM; 2) when Fe limitation is neglected, the models have similar total IPP (within 15%) as well as seasonal and regional patterns of IPP, suggesting some confidence in simulated long-term trends in integrated primary production. Including Fe limitation may lead to incomplete drawdown of macronutrients and limit overall production. The simulated long-term trends show small but persistent increases in most regions, except for a slight decrease in the Greenland Sea and fairly constant values in the Arctic Basin with large interannual variability (CMOC and both CanOE models). Interannual variability is suppressed in PISCES, likely due to the limited macronutrient uptake and suppressed growth.

The biogeochemical models are generally built on the same principles, which leads to the use of commonly applied functional dependencies and a range of parameters that are tunable within some reasonable range. Ideally parameter ranges are determined based on observations within the model region, but this is not always possible. Parameterizations derived from observations in other regions may not be applicable in the Arctic. In this study, a range of parameter values was tested with the intent to improve simulation of the SCM, but with limited success. For example, changing the linear and quadratic mortality of phytoplankton and zooplankton and light-saturated growth rates in phytoplankton affects the depth and intensity of the SCM in CanOE, but a pattern similar to CMOC required values outside the acceptable range.

The key differences among the CanOE/CanOE-CSIB, CMOC, and PISCES models were identified as the treatment of dissolved inorganic nitrogen and its uptake by phytoplankton, the light attenuation, including chlorophyll-dependent light absorption parameterization, and multiple detrital sinking rates in higher complexity models:

1) CanOE and PISCES have a more complex N cycle than CMOC. In CanOE, NO3 cannot be consumed if NH4 is present. Remineralization to NH4 can greatly affect the depth distribution of phytoplankton and chlorophyll independent of NO3 concentration. PISCES contains multiple

nutrient limitation of phytoplankton growth, and Fe limitation seems to trigger the development of an SCM despite the availability of N.

2) While CMOC uses a single-band (PAR) light attenuation scheme, CanOE and PISCES use a more realistic bio-optical model with three wavelength bands. All models consider local chlorophyll concentrations but only PISCES uses phytoplankton size-dependent absorption. CMOC, however, produces the most realistic SCM with the simplest and least physically realistic attenuation scheme.. Further investigation of optical characteristics of the Arctic marine environment (e.g., attenuation dependence on wavelength and on other absorbing substances such as CDOM) are warranted.

3) Detrital sinking rates affecting the depth of nutrient remineralization also affect the SCM depth. While tuning of these rates has similar limitations as tuning mortality and growth, the key difference is that a more complex community structure allows for the multiple sinking rates.

Based on this analysis the following recommendations can be made: 1. adjustments within an acceptable range to parameters such as linear and/or quadratic mortality rates of phytoplankton and zooplankton, photosynthetic growth rate, and detrital sinking and remineralization can be made to improve simulated vertical distribution of chlorophyll (these changes can be focused preferentially on small phytoplankton, which contribute the most to the bloom); 2. gaining better understanding of the taxonomy, size distribution and species-specific properties of Arctic phytoplankton would allow us to tune e.g. the nutrient uptake and photoadaptation parameters more specifically for the Arctic environment; 3. including micronutrient (e.g. Fe) limitation in models, , may lead to differences in total integrated PP, i.e. if the available Fe does not allow macronutrients to be fully utilized. Models with Fe limitation developed for the global domain or mid-latitude regions should be applied with caution in the Arctic, and further research on Arctic and subarctic Fe sources and cycling is warranted.

Acknowledgements

The publication contributes to the model intercomparison efforts of the Forum for Arctic Modeling and Observational Synthesis (FAMOS), Biogeochemical exchange processes at sea-ice interfaces (BEPSII) and the European Union's Horizon 2020 research and innovation programme under grant agreement No 101003826 via project CRiceS (Climate Relevant interactions and feedbacks: the key role of sea ice and Snow in the polar and global climate system). The work has been funded by Fisheries and Oceans Canada via the Aquatic Climate Change Adaptation Services Program (ACCASP) and Environment and Climate Change Canada.

Data access

Code for both FABM/CanOE and FABM/CMOC is available at:
https://sourceforge.net/u/oliviergjriche/fabm

Code for both Beaufort case is available at:

https://sourceforge.net/u/oliviergjriche/gotm_cases

Some of the code for the experiment matrices and the visualization is available at:

https://sourceforge.net/u/oliviergjriche/extras

Observations DFO data archive:

DFO (2024). Institute of Ocean Sciences Data Archive. Ocean Sciences Division. Department of Fisheries and Oceans Canada. **http://www.pac.dfo-mpo.gc.ca/science/oceans/data-donnees/index-eng.html**. Data obtained on 2018/05/22.

REFERENCES

Abraham, C., Steiner, N. Monahan, A. and Michel, C. 2015. Effects of subgrid-scale snow thickness variability on radiative transfer in sea ice., J. Geophys. Res. Oceans, 120 (8), 5597-5614, doi:10.1002/2015JC010741.

Antoine D., Hooker, S.B., Bélanger, S., Matsuoka A., Babin M. 2013. Apparent optical properties of the Canadian Beaufort Sea – Part 1: Observational overview and water column relationships. Biogeosciences 10, 4493-4509. doi:10.5194/bg-10-4493-2013.

Ardyna, M., Babin, M. Gosselin, M. Devred, E., Bélanger, S., Matsuoka, A., Tremblay, J.-E. 2013. Parameterization of vertical chlorophyll a in the arctic ocean: impact of the subsurface chlorophyll maximum on regional, seasonal, and annual primary production estimates, Biogeosciences, 10 (4383-4404), doi:10.5194/bg-10-4383-2013.

Ardyna, M., Babin, M., Gosselin, M., Devred, E., Rainville, L., and Tremblay, J.-É. 2014. Recent Arctic Ocean sea ice loss triggers novel fall phytoplankton blooms, *Geophys. Res. Lett.*, 41, 6207– 6212, doi:10.1002/2014GL061047.

Arora, V.K., Boer, G.J., Christian, J.R., Curry, C.L., Denman, K.L., Zahariev, K., Flato, G.M., Scinocca, J.F., Merryfield, W.J., Lee, W.G. 2009. The effect of terrestrial photosynthesis down-regulation on the 20th century carbon budget 1110 simulated with the CCCma Earth System Model. J. Clim. 22, 6066-6088. doi: https://doi.org/10.1175/2009JCLI3037.1.

Arrigo, K., van Dijken G. 2011. Secular trends in Arctic Ocean net primary production, Journal of Geophysical Research: Oceans, 116 (C9), doi: 10.1029/2011JC007151.

Arrigo, K., van Dijken, G. 2015. Continued increases in Arctic Ocean primary production, Progress in Oceanography, 136, 60-70, doi: 10.1016/j.pocean.2015.05.002.

Aumont, O., Ethé, C., Tagliabue, A., Bopp, L., Gehlen, M. 2015. PISCES-v2: an ocean biogeochemical model for carbon and ecosystem studies, Geosci. Model Dev., 8, 2465-2513, doi:10.5194/gmd-8-2465-2015.

Balmaseda, M., Mogensen, K., Weaver, A. 2013. Evaluation of the ECMWF ocean reanalysis system ORAS4, Quarterly Journal of the Royal Meteorological Society, 139 (674), 1132-1161.

Berge, J., Renaud P.E., Darnis, G., Cottier, F., Last, K., Gabrielsen, T.M., Johnsen, G., Seuthe, L. et. al., In the dark: A review of ecosystem processes during the Arctic polar night, Progress in Oceanography, pp. 258-271, https://doi.org/10.1016/j.pocean.2015.08.00, 2015.

Bricaud, A., Babin, M., Morel, A., Claustre, H. 1995. Variability in the chlorophyll-specific absorption coefficients of natural phytoplankton: analysis and parameterization, J. Geophys. Res., 100, 13321–13332, https://doi.org/10.1029/95JC00463.

Brown, Z., Lowry, K., Palmer, M., van Dijken, G., Mills, M., Pickart, R., Arrigo, K., 2015. Characterizing the subsurface chlorophyll a maximum in the Chukchi Sea and Canada Basin,

Deep Sea Research Part II: Topical Studies in Oceanography, Volume 118, Part A, Pages 88-104, https://doi.org/10.1016/j.dsr2.2015.02.010.

Carmack, E.C., McLaughlin, F.A., Vagle, S., Melling, H., Williams, W.J. 2010. Structures and property distributions in the three oceans surrounding Canada in 2007: A basis for a long-term ocean climate monitoring strategy, Atmosphere-Ocean, 48 (4), 211-224, doi:10.3137/OC324.2010.

Christian, J.R., Arora V.K., Boer, G.J., Curry,C.L., Zahariev, K., Denman, K.L., Flato, G.M., Lee, W.G., Merryfield, W.J., Roulet, N.T., Scinocca, J.F. 2010. The global carbon cycle in the Canadian Earth System Model (CanESM1): Preindustrial control simulation, Journal of Geophysical Research, 115, doi:10.1029/2008JG000920.

Christian, J. R., Denman, K. L., Hayashida, H., Holdsworth, A. M., Lee, W. G., Riche, O. G. J., Shao, A. E., Steiner, N., Swart, N. C. 2022. Ocean biogeochemistry in the Canadian Earth System Model version 5.0.3: CanESM5 and CanESM5-CanOE, Geosci. Model Dev., 15, 4393–4424, https://doi.org/10.5194/gmd-15-4393-2022.

Cooper, L., McClelland, J., Holmes, R., Raymond, P., Gibson, J., Guay, C., Peterson, B. 2008. Flow-weighted values of runoff tracers ($\delta_{18}O$, DOC, Ba, alkalinity) from the six largest Arctic rivers, Geophysical Research Letters, 35 (18).

Dai, A., Trenberth, K.E. 2002. Estimates of Freshwater Discharge from Continents: Latitudinal and Seasonal Variations. J. Hydrometeor., **3**, 660–687.

Dai, A., Qian, T., Trenberth, K., Milliman, J.D. 2009. Changes in continental freshwater discharge from 1948-2004, J. Climate, 22, 773-2791.

Dupont, F., Higginson, S., Bourdall-Badie, R., Lu, Y., Roy, F., Smith, G., Lemieux, J.-F., Garric, G., Davidson, F. 2015. A high-resolution ocean and sea-ice modelling system for the Arctic and North Atlantic oceans, Geosci. Model Dev., 8 (5), 15771594.

Dussin, R., Barnier, B., Brodeau, L., Molines J. 2016. The making of the Drakkar forcing set DFS5, Tech. Rep. 01-04,16, DRAKKAR/MyOcean.

Frey, K.E., Comiso, J.C. , Cooper, L.W., Grebmeier, J.M., Stock, L.V. 2016. Arctic ocean primary productivity: The response of marine algae to climate warming and sea ice decline. Arctic report card, https://www.arctic.noaa.gov/Report-Card/Report-Card-2018/ArtMID/7878/ArticleID/778/Arctic-Ocean-Primary-Productivity-The-Response-of-Marine-Algae-to-Climate-Warming-and-Sea-Ice-Decline.

Garçon, V., Bell, T., Wallace, D., Arnold, S., Baker, A. Bakker, D., Bange, H., Bates, N., Bopp, L., Boutin, J., Boyd, P., Bracher, A., Burrows, J., Carpenter, L., de Leeuw, G., Fennel, K., Font, J., Friedrich, T., Garbe, C., Gruber, N., Jaegle, L., Lana, A., Lee, J., Liss, P., Miller, L., Olgun, N., Olsen, A., Pfeil, B., Quack, B., Read, K., Reul, N., Rödenbeck, C., Rohekar, S., Saiz-Lopez, A., Saltzman, E., Schneising, O., Schuster, U., Seferian, R., Steinhoff, T., Traon, P.-Y. L., Ziska, F. 2014. Ocean-Atmosphere Interactions of Gases and Particles, Chapter: Perspectives and Integration in SOLAS Science, Springer Earth System Science, doi:10.1007/978-3-642-25643-1.

Geider R.J., MacIntyre H.L., Kana T.M. 1996. A dynamic model of photoadaptation in phytoplankton. Limnol Oceanogr 41:1-15.

Geider, R.J., MacIntyre, H.L., Kana, T.M. 1997. Dynamic model of phytoplankton growth and acclimation: responses of the balanced growth rate and the chlorophyll a:carbon ratio to light, nutrient-limitation and temperature., Marine Ecology Progress Series, 148 (1-3), 187-200, doi:10.3354/meps148187.

Hayashida, H. 2018. Modelling sea-ice and oceanic dimethylsulfide production and emissions in the Arctic, Ph.D. thesis, University of Victoria, http://dspace.library.uvic.ca/handle/1828/10486.

Hayashida, H., Christian, J., Holdsworth, A., Hu, X., Monahan, A., Mortenson, E., Myers, P. Riche, O., Sou, T., Steiner, N. 2019. CSIB v1: a sea-ice biogeochemical model for the NEMO community ocean modelling framework, Geosci. Model Dev., 12, 5,1965-1990, https://doi.org/10.5194/gmd-12-1965-2019.

Hill, V.J., Matrai, P.A., Olson, E., Suttles, S., Steele, M., Codispoti, L.A., Zimmerman, R.C. 2013. Synthesis of integrated primary production in the Arctic Ocean: II. In situ and remotely sensed estimates, Progress in Oceanography, Volume 110, Pages 107-125, https://doi.org/10.1016/j.pocean.2012.11.005.

Holmes, R.M., McClelland, J.W., Peterson, B.J. , Tank, S., Bulygina, E., Eglington, T.I, Gordeev, V.V. , Gurtovaya, T.Y., Raymond, P.A., Repeta, D.J., Staples, R.S., Striegl, R.G., Zhulidov A.V., Zimov, S.A. 2012. Seasonal and Annual Fluxes of Nutrients and Organic Matter from Large Rivers to the Arctic Ocean and Surrounding Seas. Estuaries and Coasts **35**, 369–382. https://doi.org/10.1007/s12237-011-9386-6.

Hood, R.R., Christian, J.R. 2008. Chapter 33 - Ocean Nitrogen Cycle Modeling, Editor(s): Douglas G Capone, Deborah A Bronk, Margaret R Mulholland, Edward J Carpenter, Nitrogen in the Marine Environment (Second Edition), Academic Press, Pages 1445-1495, ISBN 9780123725226, https://doi.org/10.1016/B978-0-12-372522-6.00033-5.

Hu, X., Myers, P. 2013. A Lagrangian view of Pacific water inflow pathways in the Arctic Ocean during model spin-up, Ocean Modelling, 71, 66-80, doi:10.1016/j.ocemod.2013.06.007.

Hu, X., Myers, P. 2014. Changes to the Canadian Arctic Archipelago sea ice and freshwater Fluxes in the 21st century under the IPCC A1B climate scenario., Atmosphere-Ocean, 52, 331-350, doi:10.1080/07055900.2014.942592.

Jin, M., Deal, C., Lee, S., Elliott, S., Hunke, E., Maltrud, M., Jeffery, N. 2012. Investigation of Arctic sea ice and ocean primary production for the period 1992-2007 using a 3-d global ice-ocean ecosystem model, Deep Sea Res. II, 81, 28-35, doi: 10.1016/j.dsr2.2011.06.003.

Jin, M., Popova, E., Zhang, J., Ji, R., Pendleton, D., Varpe, Ø., Yool, A., Lee, Y. 2016. Ecosystem model intercomparison of under-ice and total primary production in the Arctic Ocean, J. Geophys. Res. Oceans, 121, 934-948, doi:10.1002/2015JC011183.

Kana T.M., Glibert P.M. 1987. Effect of irradiances up to 2000 μE $m^{-2}s^{-1}$ on marine Synechococcus WH7803-II. Photosynthetic responses and mechanisms. Deep Sea Res 34:497-516.

Kirtman, B., Power, S., Adedoyin, J., Boer, G., Bojariu, R., Camilloni, I. Doblas-Reyes, F., Fiore, A., Kimoto, M., Meehl, G., Prather, M., Sarr, A., Schar, C., Sutton, R., van Oldenborgh, G. Vecchi, G., Wang, H. 2013. Climate Change 2013: The Physical Science Basis. Contribution of Working Group I to the Fifth Assessment Report of the Intergovernmental Panel on Climate

Change, Chapter: Near-term Climate Change: Projections and Predictability, Cambridge University Press, United Kingdom and New York, NY, USA.

Lee, Y. J., Matrai, P., Friedrichs, M., Saba, V., Antoine, D., Ardyna, M. et. al. 2015. An assessment of phytoplankton primary productivity in the Arctic Ocean from satellite ocean color/in situ chlorophyll-a based models, J. Geophys. Res. Oceans, 120, 6508-6541, doi:10.1002/2015JC011018.

Madec, G. 2008. Nemo reference manual, ocean dynamic component: NEMO-OPA, Tech. Rep. 27, Note du Pole de modélisation, Institut Pierre Simon Laplace, ISSN No.1288-1619.

Martin, J., Tremblay, J.-E. , Gagnon, J., Tremblay, G., Lapoussiére, A., Jose, C., Poulin, M., Gosselin, M., Gratton, Y., Michel, C. 2010. Prevalence, structure and properties of subsurface chlorophyll maxima in Canadian Arctic water, Mar Ecol Prog Ser, 412, 69-84, doi:10.3354/meps08666.

Matrai, P., Olson, E., Suttles, S., Hill, V., Codispoti, L., Light, B., Steele, M. 2013. Synthesis of primary production in the Arctic Ocean: I. surface waters, 1954-2007, Prog Oceanogr, 110, 93-106.

McClelland, J., Holmes, R., Dunton, K., Macdonald, R. 2012. The Arctic Ocean estuary, Estuaries and Coasts, 35 (2), 353-368.

Morel, A., Maritorena, S. 2001. Bio-optical properties of oceanic waters: A reappraisal, J. Geophys. Res. Oceans, 106 (C4), 7163-7180.

Mortenson, E., Hayashida, H., Steiner, N., Monahan, A., Blais, M., Gale, M. A. , Galindo, V., Gosselin, M., Hu, X., Lavoie, D., Mundy, C.J. 2017. A model-based analysis of physical and biological controls on ice algae and pelagic primary production in Resolute passage, Elem Sci Anth., 5 (39), doi: http://doi.org/10.1525/elementa.229.

Mortenson, E., Steiner, N., Monahan, A.H., Hayashida, H., Sou, T., Shao, A. 2020. Modeled impacts of sea ice exchange processes on Arctic Ocean carbon uptake and acidification (1980–2015). Journal of Geophysical Research: Oceans, 125, e2019JC015782. https://doi.org/10.1029/2019JC015782.

Mundy, C., Gosselin, M., Ehn, J., Gratton, Y., Rossnagel, A., Barber, D., Martin, J., Tremblay, J.-E., Palmer, M., Arrigo, K., Darnis, G., Fortier, L., Else, B., Papakyriakou, T. 2009. Contribution of under-ice primary production to an ice-edge upwelling phytoplankton bloom in the Canadian Beaufort Sea, Geophys.Res. Lett., 36 (L17601), doi:10.1029/2009GL038837.

Parker, R. 1993. Dynamic models for ammonium inhibition of nitrate uptake by phytoplankton, Ecological Modelling, 66, 113-120, doi:10.1016/0304-3800(93)90042-Q.

Popova, E., Yool, A., Coward, A., Dupont, F., Deal, C., Elliott, S., Hunke, E., Jin, M., Steele, M., Zhang, J. 2012. What controls primary production in the arctic ocean? Results from an intercomparison of five general circulation models with biogeochemistry., J Geophys Res, 117 (C00D12), doi: 10.1029/2011JC007112.

Rijkenberg, M.J.A., Slagter, H.A., Rutgers van der Loeff, M., van Ooijen J., Gerringa L.J.A. 2018. Dissolved Fe in the deep and upper Arctic Ocean with a focus on Fe limitation in the Nansen Basin. Front. Mar. Sci. 5:88. doi: 10.3389/fmars.2018.00088.

Sakshaug, E. 2004. The Organic Carbon Cycle in the Arctic Ocean, chap. Primary and secondary production in the Arctic seas, pp. 57-81, Springer Publishing Company, Heidelberg, Germany.

Steiner, N., Sou, T., Deal, C., Jackson, J., Jin, M., Popova, E., Williams, W., Yool, A. 2015. The future of the subsurface chlorophyll-a maximum in the Canada Basin - a model intercomparison, JGR Oceans, 121 (1), 387-409.

Swart, N.C., Cole, J.N.S., Kharin, V.V., Lazare, M., Scinocca, J.F., Gillett, N.P., Anstey, J., Arora, V., Christian, J.R., Hanna, S., Jiao, Y., Lee, W.G., Majaess, F., Saenko, O.A., Seiler, C., Seinen, C., Shao, A., Sigmond, M., Solheim, L., von Salzen, K., Yang, D., Winter, B. 2019. The Canadian Earth System Model version 5 (CanESM5.0.3), Geosci. Model Dev., 12, 4823–4873, https://doi.org/10.5194/gmd-12-4823-2019.

Tank, S.E., Raymond, P.A., Striegl, R.G., McClelland, J.W., Holmes, R.M., Fiske, G.J., Peterson, B.J. 2012. A land-to-ocean perspective on the magnitude, source and implication of DIC flux from major Arctic rivers to the Arctic Ocean, Global Biogeochemical Cycles, 26 (GB4018), doi:10.1029/2011GB004192.

Tian, R. 2006. Toward standard parametrizations in marine biological modeling, Ecological Modelling, 193, 363-386, doi:10.1016/j.ecolmodel.2005.09.003.

Tremblay, J.-E., Simpson, K., Martin, J., Miller, L., Gratton, Y, Barber, D., Price, N.M. 2008. Vertical stability and the annual dynamics of nutrients and chlorophyll fluorescence in the coastal southeast Beaufort Sea, J. Geophys. Res., 113, C07S90, doi:10.1029/2007JC004547.

Umlauf, L., Burchard, H. 2005. Second-order turbulence closure models for geophysical boundary layers. A review of recent work, Continental Shelf Research, Volume 25, Issues 7–8, Pages 795-827, ISSN 0278-4343, https://doi.org/10.1016/j.csr.2004.08.004.

Vallina, S., Quéré, C.L. 2008. Preferential uptake of NH_4^+ over NO_3^- in marine ecosystem models: A simple and more consistent parameterization, Ecological Modelling, pp. 393-397, doi: 10.1016/ecolmodel.2008.06.038.

Vallina, S., Cermeno, P., Dutkiewicz, S., Lorea, M., Montoya, J. 2017. Phytoplankton functional diversity increases ecosystem productivity and stability, Ecological Modelling, 361, 184-196, doi:10.1016/j.ecolmodel.2017.06.020.

Vancoppenolle, M., Bopp, L., Madec, C., Dunne, J., Ilyina, T., Halloran, P., Steiner, N. 2013. Future Arctic primary productivity from CMIP5 simulations: Uncertain outcome, but consistent mechanisms, Global Biogeochemical Cycles, 27, doi:10.1002/gbc.20055.

Watanabe, E., Jin, M., Hayashida, H., Zhang, J., Steiner, N. 2019. Multi-Model Intercomparison of the Pan-Arctic Ice-Algal Productivity on Seasonal, Interannual, and Decadal Timescales. *Journal of Geophysical Research: Oceans*, 124, 9053–9084. https://doi.org/10.1029/2019JC015100

Zahariev, K., Christian, J., Denman, K. 2007. The Canadian Model of Ocean Carbon (CMOC) v1.0, CCCma, Environment Canada, https://crd-data-donnees-rdc.ec.gc.ca/CCCMA/publications/2008_Zahariev_ProgOceanogr_CanadianOceanCarbonModel/CMOCreport.pdf.

Zahariev, K., Christian, J., Denman, K. 2008. A global ocean carbon model with parameterizations of iron limitation, calcification and N_2 fixation; preindustrial, historical and fertilization simulations, Progress in Oceanography, 77 (1), 56-82.

Zhang, J., Spitz, Y., Steele, M., Ashjian, C., Campbell, R., Berline, L., Matrai, P. 2010. Modeling the impact of declining sea ice on the Arctic marine planktonic ecosystem., Journal of Geophysical Research: Oceans, 115 (C10), C10,015, doi: 10.1029/2009JC005387.

APPENDICES

Appendix 1: Supplementary figures

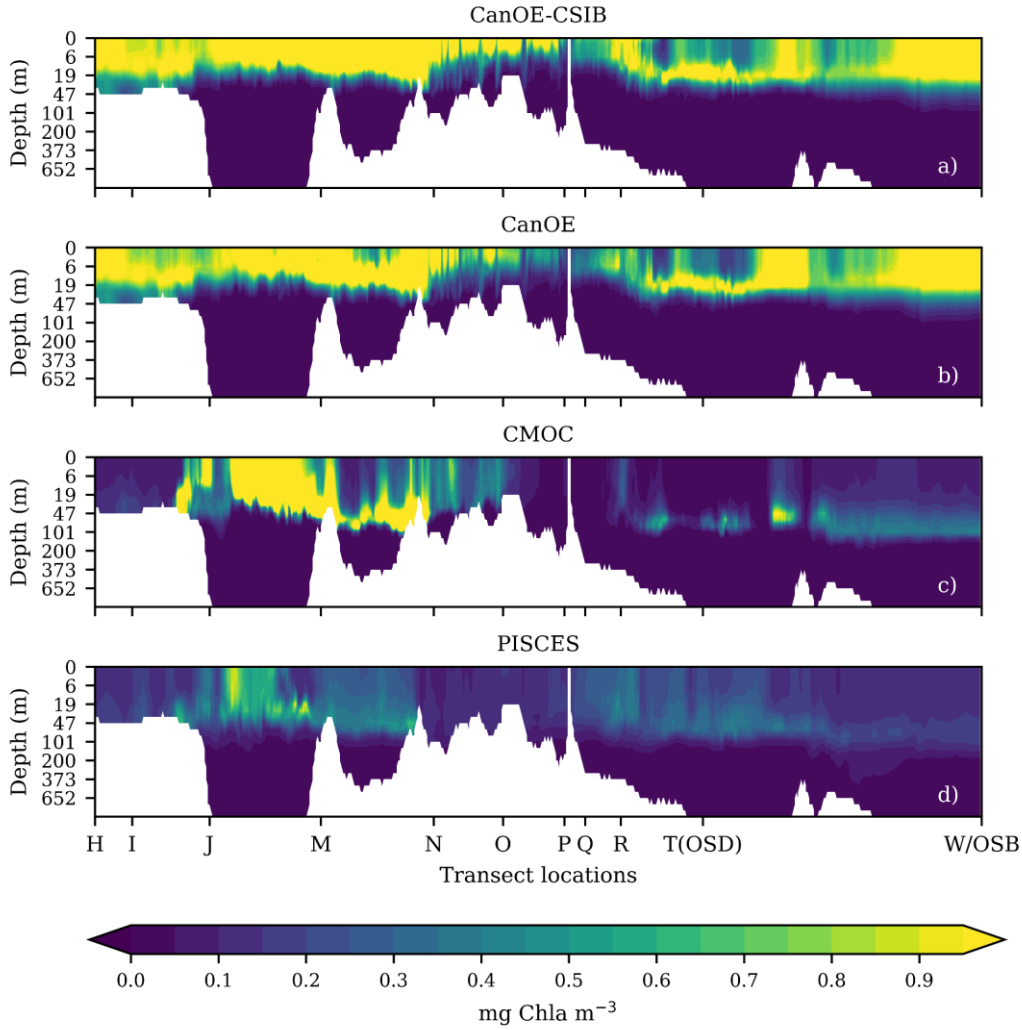

Figure S1: Simulated Chla along the C3O transect in June 2007

Simulated Chla [mg-Chla m^{-3}] for June along the C3O transect indicated in Fig. 7 for a) NAA-CanOE-CSIB, b) NAA-CanOE, c) NAA-CMOC, d) NAA-PISCES.

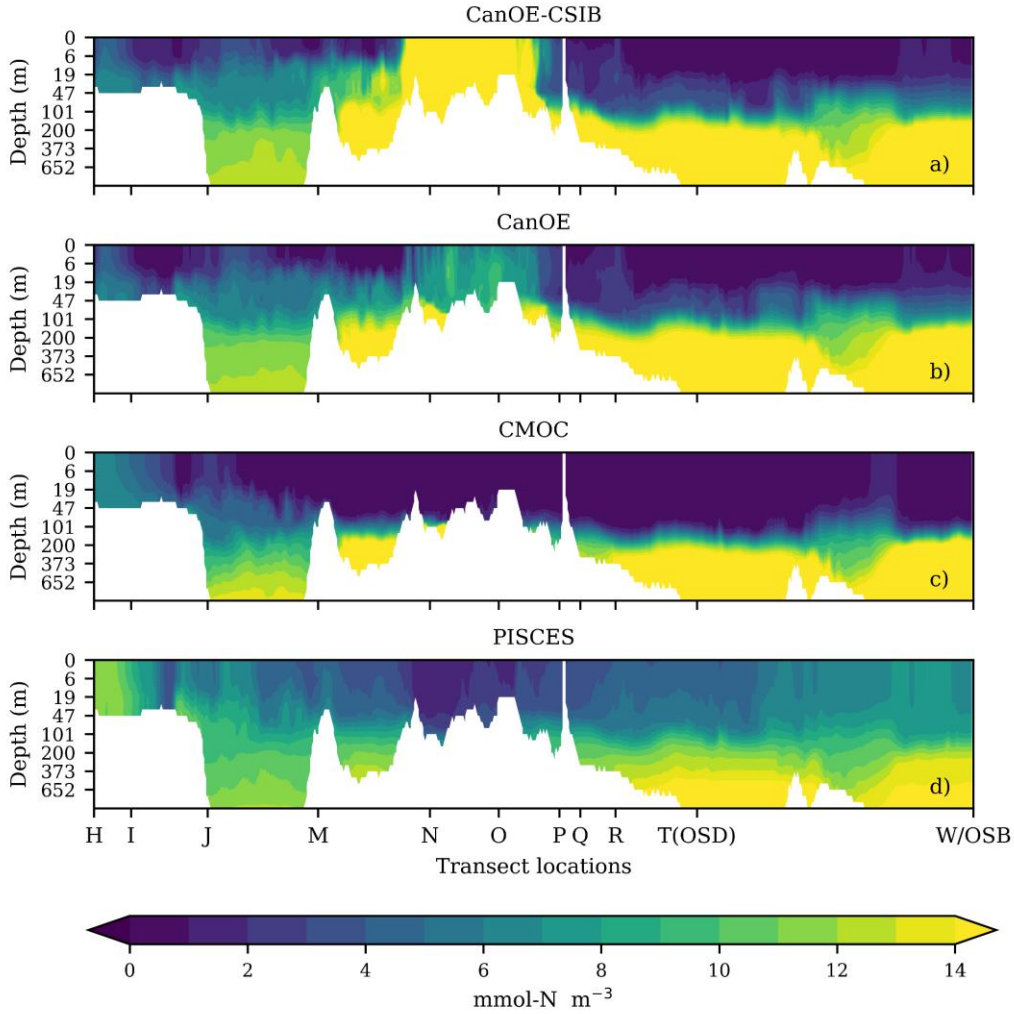

Figure S2: Simulated NO3 along the C3O transect in June 2007

Simulated NO3 [mM-N m^{-3}] for June along the C3O transect indicated in Fig. 7 for a) NAA-CanOE-CSIB, b) NAA-CanOE, c) NAA-CMOC, d) NAA-PISCES.

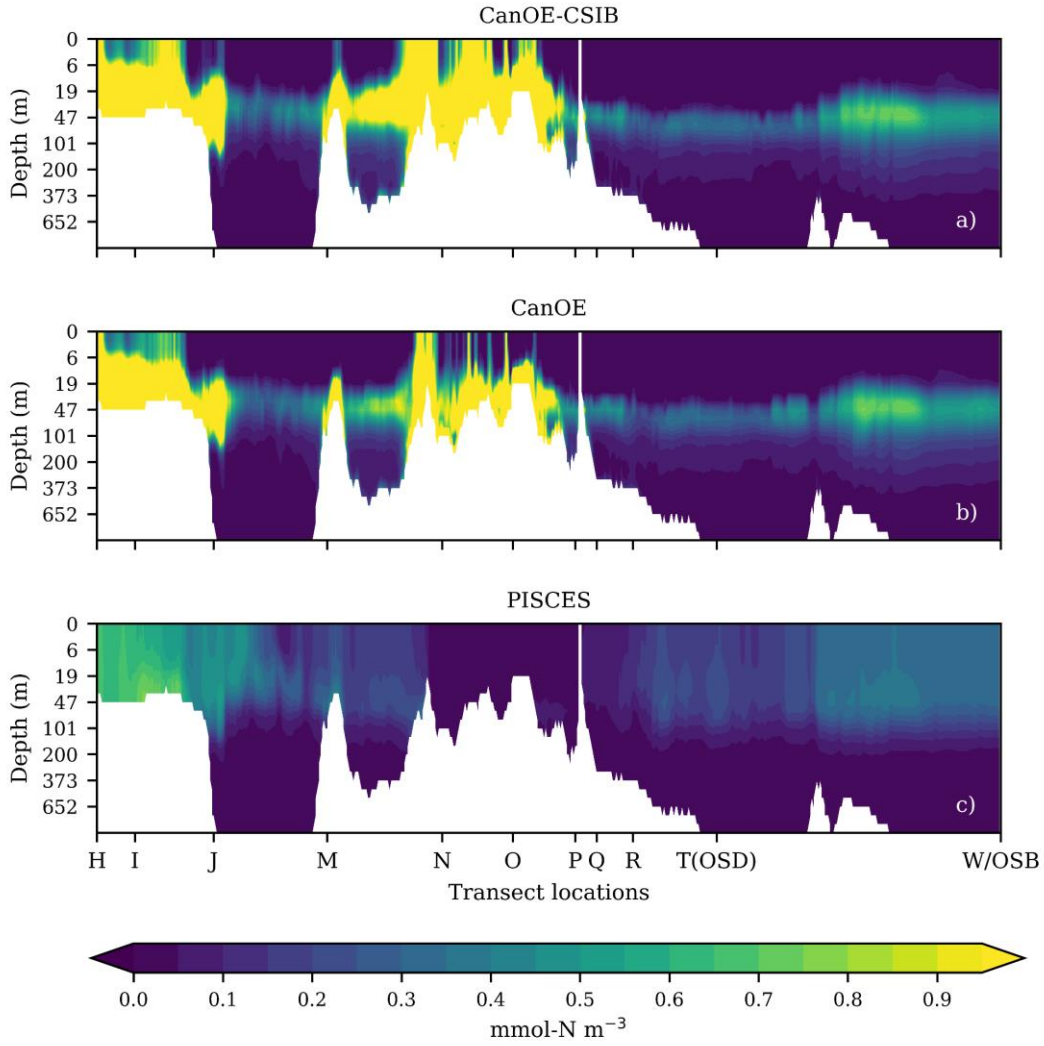

Figure S3: Simulated NH4 along the C3O transect in August 2007

Simulated Chla [mM-N m^{-3}] for August along the C3O transect indicated in Fig. 7 for a) NAA-CanOE-CSIB, b) NAA-CanOE.

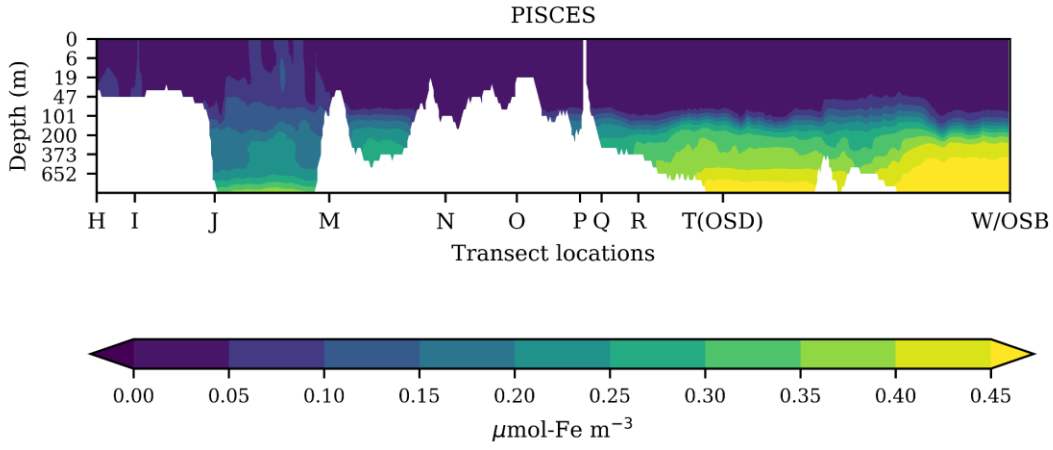

Figure S4: Simulated Iron along the C3O transect in August 2007

Simulated Iron (Fe) [µM-Fe m^{-3}] for August along the C3O transect indicated in Fig. 7 for NAA-PISCES.

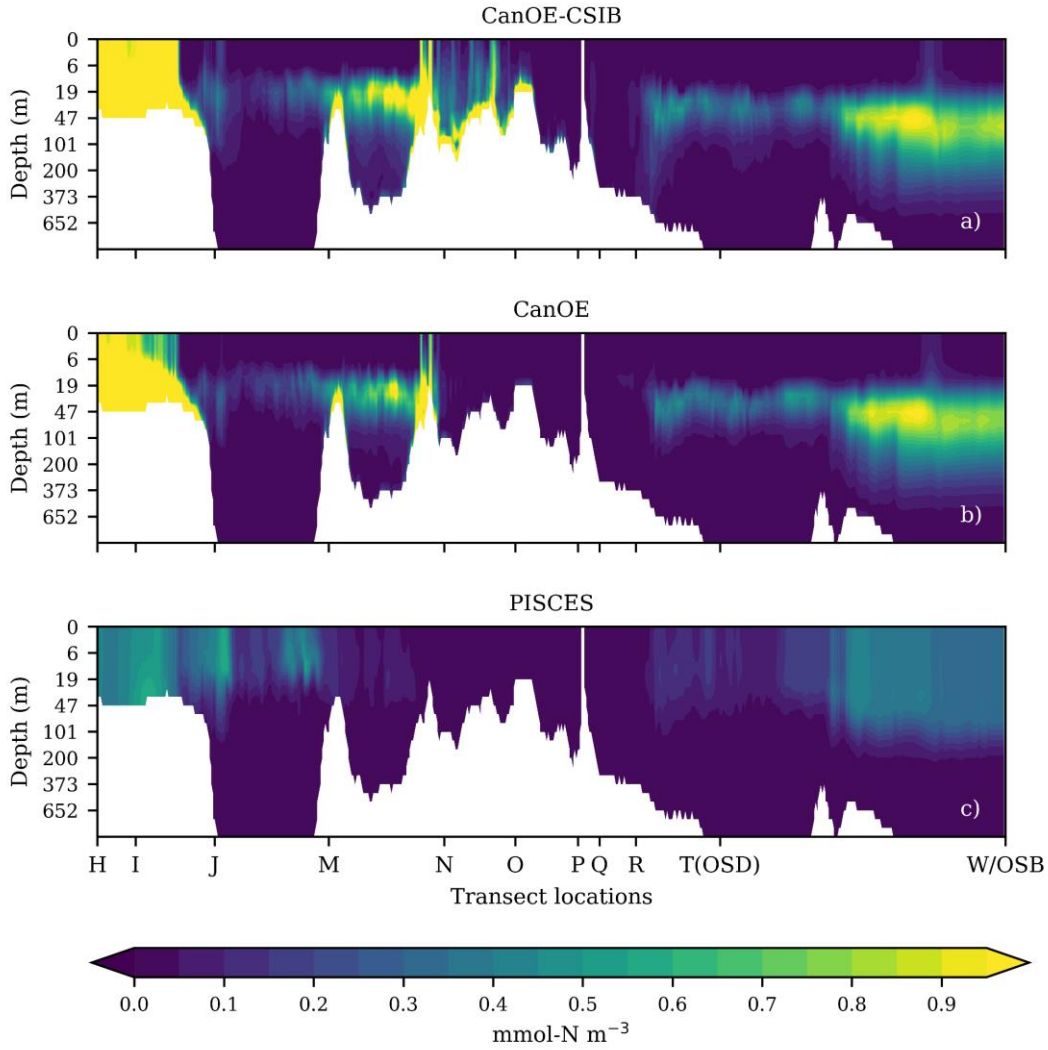

Figure S5: Simulated NH4 along the C3O transect in June 2007

Simulated Chla [mM-N m^{-3}] for June along the C3O transect indicated in Fig. 7 for a) NAA-CanOE-CSIB, b) NAA-CanOE.

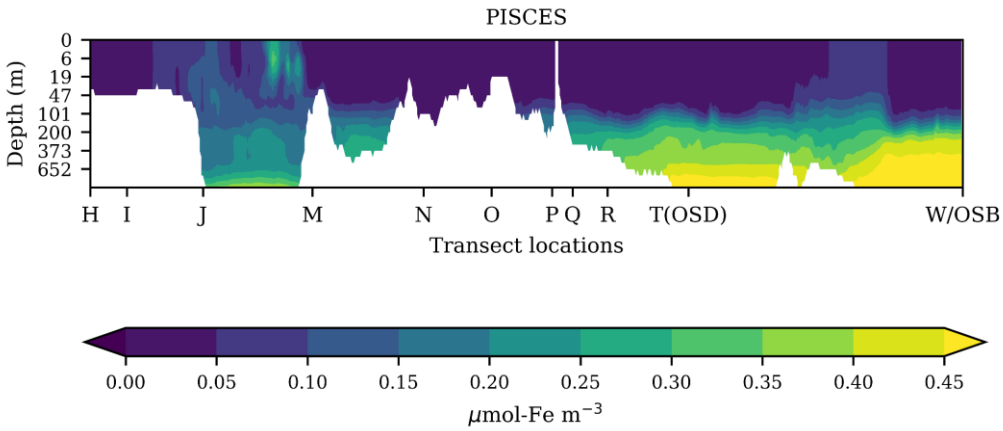

Figure S6: Simulated Iron along the C3O transect in June 2007

Simulated Iron (Fe) [μM-Fe m^{-3}] for June along the C3O transect indicated in Fig. 7 for NAA-PISCES.

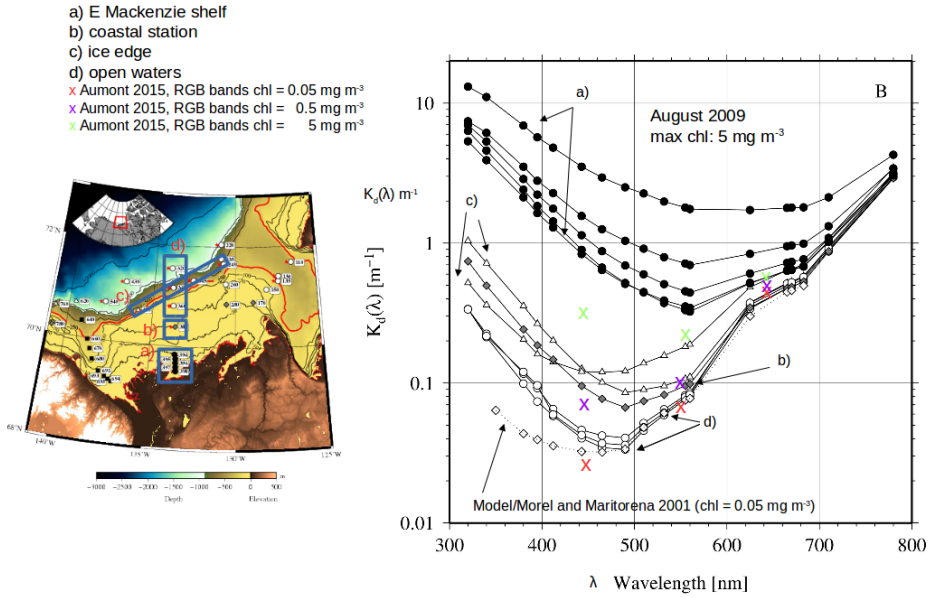

Figure S7: Observation of diffuse attenuation coefficients

Observation of diffuse attenuation coefficients in the water column of the Canada Basin [Antoine et al. 2013] with attenuation coefficients for RGB bands for 0.05, 0.5 and 5 mg m^{-3} Chla [Aumont et al, 2015].

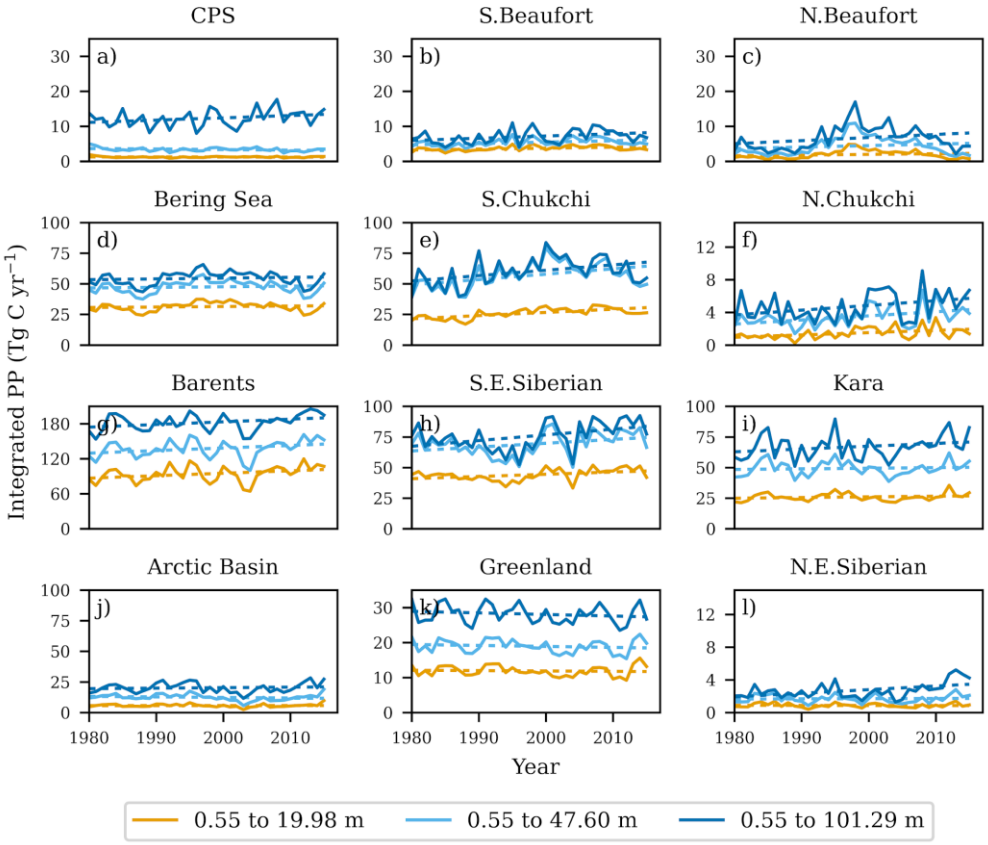

Figure S8: Simulated trends in primary production for NAA-CMOC

Simulated PP [Tg-C y^{-1}] for 1995-2010, integrated over the upper 20 m (yellow), 50 m (light blue) and 100 m (dark blue). Model results are shown for NAA-CMOC for the Arctic subregions: a) Canadian Polar Shelf (CPS), b) Southern Beaufort Sea, c) Northern Beaufort Sea, d) Bering Sea, e) Southern Chukchi Sea, f) Northern Chukchi Sea, g) Barents Sea, h) Southeast Siberian Sea, i) Kara Sea, j) Arctic Basin, k) Greenland Sea l) Northeast Siberian Sea. (Subregions are indicated in Fig.1).

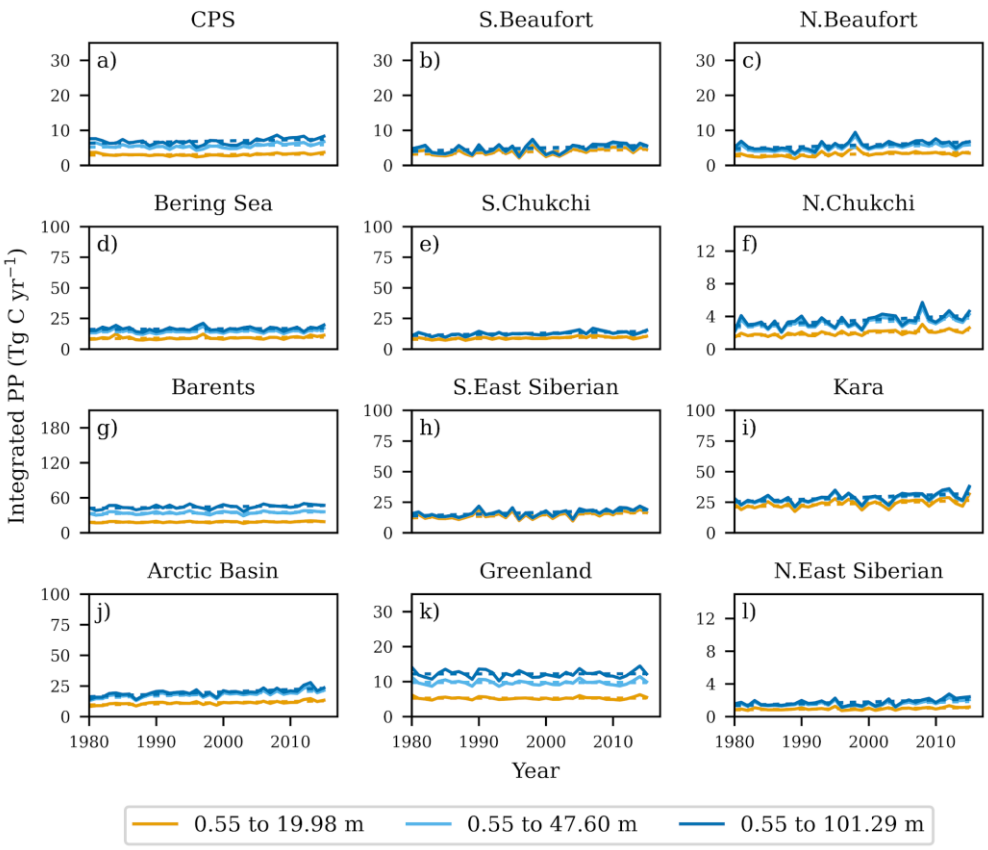

Figure S9: Simulated trends in primary production for NAA-PISCES

Simulated PP [Tg-C y^{-1}] for 1995-2010, integrated over the upper 20 m (yellow), 50 m (light blue) and 100 m (dark blue). Model results are shown for NAA-PISCES for the Arctic subregions: a) Canadian Polar Shelf (CPS), b) Southern Beaufort Sea, c) Northern Beaufort Sea, d) Bering Sea, e) Southern Chukchi Sea, f) Northern Chukchi Sea, g) Barents Sea, h) Southeast Siberian Sea, i) Kara Sea, j) Arctic Basin, k) Greenland Sea l) Northeast Siberian Sea. (Subregions are indicated in Fig.1).

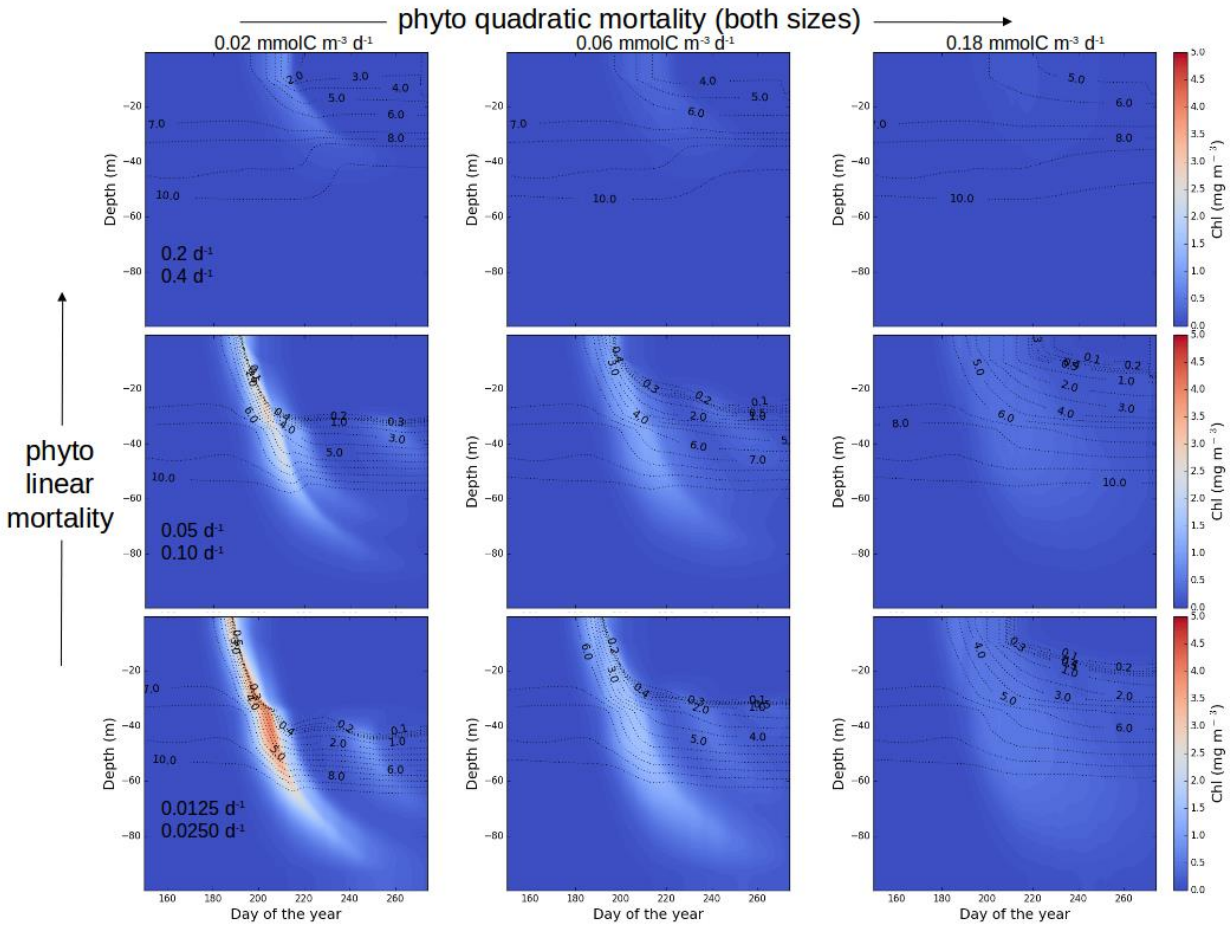

Figure S10: Simulated Chla sensitivity to mortality rates
Simulated Chla [mg-Chla m^{-3}] for sensitivity studies with the 1-d GOTM-CanOE model at the Resolute Bay location on the Canadian Polar Shelf (74ºN, 95ºW) in 2010. Results show individual and combined responses to an increase in phytoplankton quadratic mortality rate (to the right) and increasing linear mortality rate (upward). Loss of Chla is partly due to the phytoplankton mortality. The quadratic mortality rate is in fact 3 times larger in CanOE compared to CMOC. For the 1-d sensitivity study, in both CMOC and CanOE, the linear and quadratic mortality parameters are set to simultaneously affect phytoplankton and zooplankton of the same size class. Decreasing the mortality rate from the maximum value, 0.06 d^{-1} (mmol-C m^{-3})$^{-1}$ to the CMOC value of 0.015 d^{-1} (mmol-C m^{-3})$^{-1}$, with intermediate values of 0.04 and 0.02 contributes to increasing Chla to CMOC levels, around 1.4 mg-Chla m^{-3} (compared to 0.76 mg-Chla m^{-3}), the duration of the bloom is shorter. The timing of the onset of the bloom remains invariant across the values. Similar experiments with 2 size classes also lead to increased Chla levels.

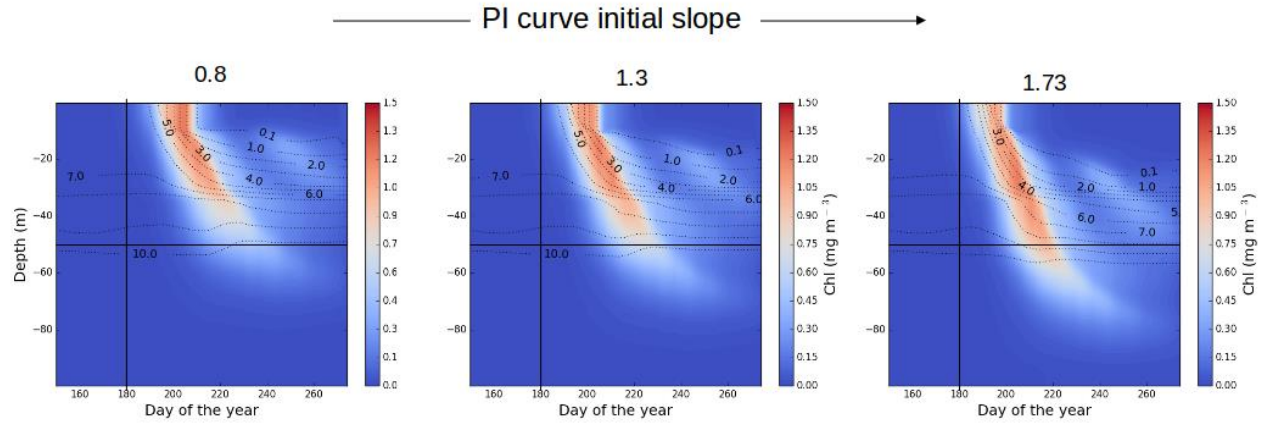

Figure S11: Simulated Chla sensitivity to PI slope
Simulated Chla [mg-Chla m^{-3}] for sensitivity studies with the 1-d GOTM-CanOE model at the Resolute Bay location on the Canadian Polar Shelf (74ºN, 95ºW) in 2010. Results show responses to an increase in the phytoplankton initial slope of the photosynthesis-irradiance (PI) curve α (to the right). Increasing α from 0.98 to 1.78 mg-C mg-$Chla^{-1}d^{-1}$ (W m^{-2})$^{-1}$ results in the reduction of the surface Chla magnitude, and a deeper SCM (either spread deeper or goes deeper below 30 m, about 50 m). The Chla-to-carbon ratio (Θ) decreases with _ from close to 0.03 mg-Chla mg-C^{-1} (maximum) around day 200 and later below 60 m (July-August) to 0.024 or less; similarly at shallower depths (above 40 m) around day 200 and later, Θ decreases from values around 0.012 or higher to values around 0.008 or higher (Θ not shown).

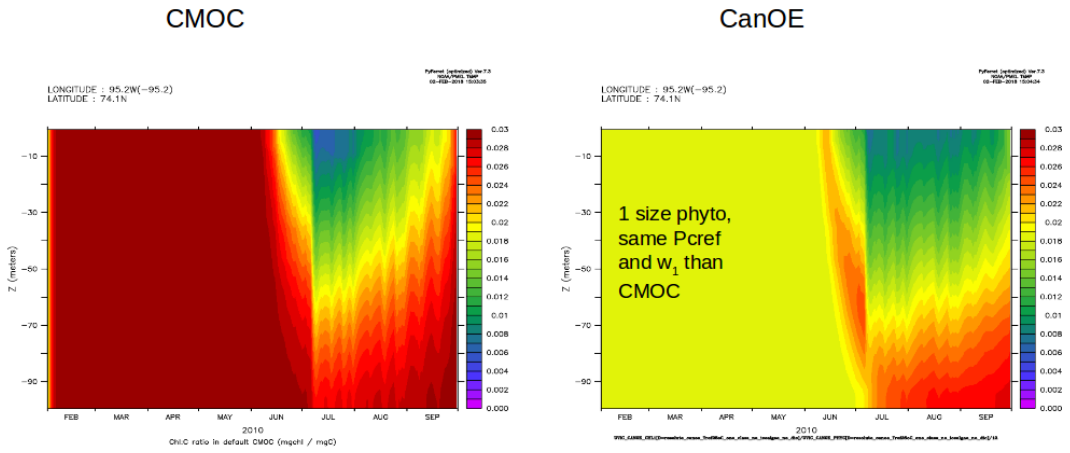

Figure S12: Modelled Chlorophyll-to-carbon ratios
SChlorophyll-to-carbon ratios (θ in mg-Chla mg-C^{-1}, maximum 0.03) for CMOC (left) and a simplified CanOE (right) for the 2010 Resolute simulation in GOTM.

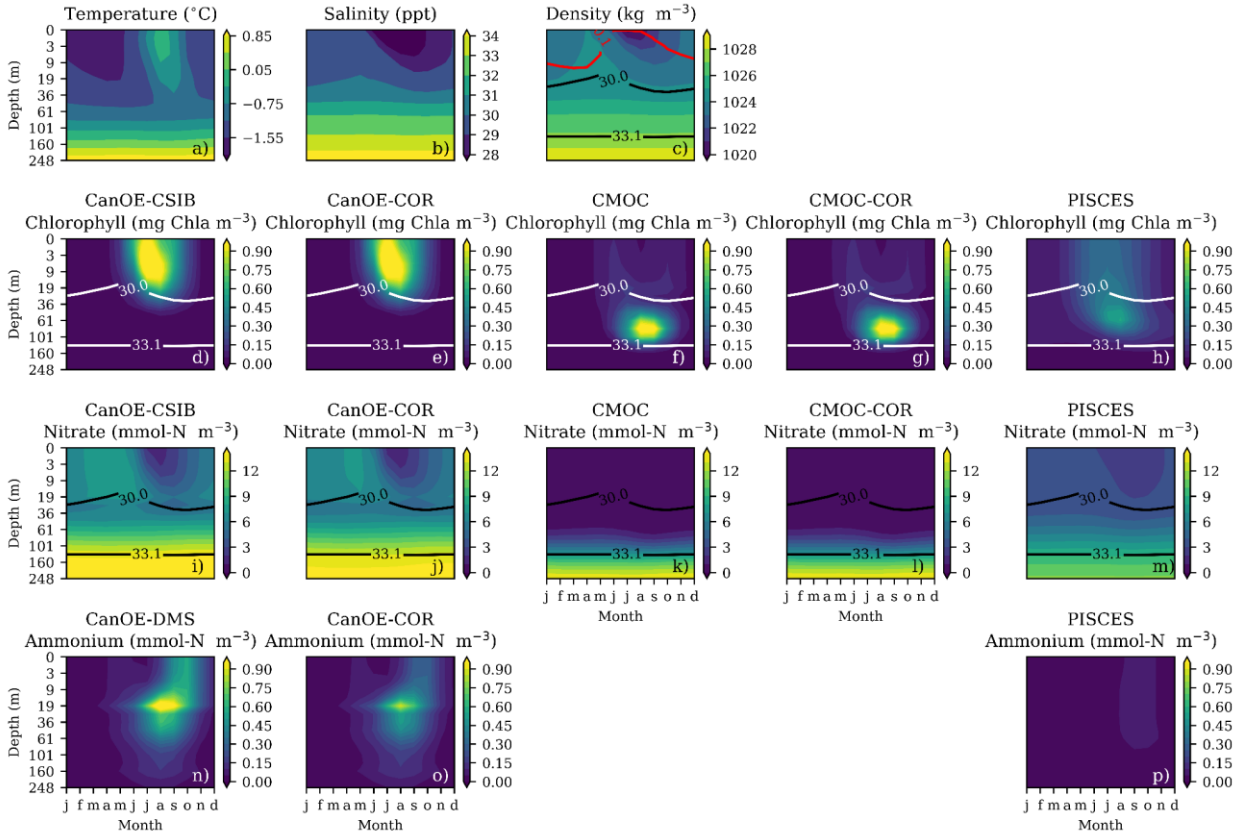

Fig. S13 Simulated seasonal cycle intercomparison for the CPS region
Simulated seasonal cycle averaged over the 1995-2010 climatology for the Canadian Polar Shel (CPS): a) Temperature, b) salinity and c) density for the NAA-CanOE-CSIB (EM300) run. Simulated Chla (2nd panel), nitrate (3rd panel) and ammonium (4th panel, no ammonium in CMOC) for CanOE-CSIB (EM300), CanOE (G510.00), CMOC with standard LIM light transmission (cmoc07.2.exp06), CMOC with adjusted light transmission (cmoc07.2.06.exp01), PISCES (PISCES.exp01, with standard LIM light transmission).

Appendix 2: Supplementary model run information

Details on model names and locations:

NAA-CanOE-CSIB
Internal run name: EM300
Output location: AEOLUS:/home/eric/from_graham_300

NAA-CanOE
Internal run name : EM303
Output location: AEOLUS:/home/eric/3d_output/EXP303/

NAA-CMOC
Internal run name : cmoc072.exp06
Output location: CEDAR:/home/tessaou/projects/def-steinern/tessaou/canoe-dms.version5/CONFIG/cmoc07.2/EXP06

NAA-PISCES
Internal run name : pisces.exp01
Output location: CEDAR:/home/tessaou/projects/def-steinern/tessaou/output_NAA/pisces/EXP01

CMOC with adjusted light transmission
Internal run name : cmoc07.2.06.exp01
Output location:
CEDAR:/home/tessaou/projects/def-steinern/tessaou/output_NAA/cmoc07.2.06/EXP01

Appendix 3: Supplementary Tables

Table S1. Summary of Ecosystem model parameters

Model		**CanOE**	**CMOC**	**PISCES**
References		Christian [2022]	Zahariev et al. [2008]	Aumont et al. [2015]
Parameter	**Units**			
Nutrient half-saturation constants[a]				
Kno3 small phyto	µM	0.1	0.1	0.13
Kno3 large phyto	µM	0.5	-	0.39
Knh4 small phyto	µM	0.05	-	0.013
Knh4 large phyto	µM	0.05	-	0.39
Kpo4 small phyto	µM	-	-	0.8
Kpo4 large phyto	µM	-	-	2.4
KFe small phyto	nM	0.1	-	1
KFe large phyto	nM	0.2	-	3
Redfield Ration C:N		6.6	7.6	variable
Phytoplankton param.				
temperature dependence type		Arrhenius eq.	Arrhenius eq.	Eppley eq.[a]
Tref reference temp	K	298.15	303.15	273.15
Activation energy growth	kJ mol^{-1}	37.4	33.26	-
Activation energy remin.	kJ mol^{-1}	54	45.73	-
Ref. rate Photosynth.	gC gC^{-1} d^{-1}	3	3	0.6
Temp. dep. at 5°C	d^{-1}	1.01b	0.92	0.83
Theta max	mgchl mgC^{-1}	0.03	0.03	0.033/0.05
Initial slope P-I curve	mgC $mgchl^{-1}$ (W m^{-2} d) $^{-1}$	7.2	5	2
Phyto small mort.	d^{-1}	0.05	0.05	0.01
Phyto large mort.	d^{-1}	0.1	-	0.01
Small quad. phyto mort.	d^{-1} (mol-C L^{-1}) $^{-1}$	0.06	0.02	0.01
Large quad. phyto mort.	d^{-1} (mol-C L^{-1}) $^{-1}$	0.06	-	0.03
Detritus parameters				
POC remin	d^{-1}	0.25	0.15	0.025
Calcite variable	µM	prognostic	diagnostic	prognostic
Rain ratio (PIC:POC)	-	0.05	0.085	0.16
PIC redissolution depth	m	2700	2700	-
POC sinking	m d^{-1}	2	8	2
Large POC sinking	m d^{-1}	30	-	30
PIC sinking	m d^{-1}	20	-	-
Zooplankton parameters				
Small zoo mort	d^{-1}	0.05	0.05	0.03
Large zoo mort.	d^{-1}	0.1	-	0.005
Small zoo exud.	d^{-1}	prognostic	0.2	0.03
large zoo exud	d^{-1}	prognostic	-	0.005
Small zoo graz.	d^{-1}	1.7	2	3
Large zoo graz.	d^{-1}	0.85	-	0.7 0.75???
Small zoo quad. mort.	d^{-1} (mol-C L^{-1}) $^{-1}$	0.06	0.02	0.0
Large zoo quad. mort.	d-1 (mol-C L-1)-1	0.06	-	0.03

[a] Eppley's equation, exponential base 1.066, values are smaller than CMOC's Arrhenius dependence for temperatures below 12.5°C This is small but significant for temperatures smaller than 2°C (e.g. between 13-20% smaller than CMOC; 15-20% smaller than CanOE for temperatures up to 10°C).

[b] $0.6 \times 1.066^{5} = 0.83$

Table S2. Integrated primary production statistics per model

Statistics of simulated pelagic primary production integrated over the top 100 m of the water column for spring (AMJ) and summer (JAS). Units are in Tg-C yr^{-1} (To obtain the total PP for the given quarter year, the value needs to be divided by 4). Indicated are mean, trend, standard deviation (STDEV), **R2 and P-value from 1980 to 2015 for NAA-CanOE-CSIB, NAA-CMOC and NAA-PISCES. (Trends are significant at the 95% level for P-values < 0.05)

Region	Season	Mean			Trend			StDev			R2			PValue		
		Canoe-CSIB	CMOC	PISCES	Canoe-CSIB	CMOC	PISCES	Canoe-CSIB	CMOC	PISCES	Canoe-CSIB	CMOC	PISCES	Canoe-CSIB	CMOC	PISCES
Arctic Basin	AMJ	31.18	27.74	26.16	0.88	0.17	0.3	0.15	0.09	0.07	0.49	0.09	0.39	0.0	0.07	0.0
	JAS	99.01	52.71	52.01	-0.02	-0.01	0.47	0.29	0.19	0.09	0.0	0.0	0.44	0.95	0.95	0.0
Baffin Bay	AMJ	57.7	40.59	25.43	-0.22	-0.28	0.02	0.12	0.1	0.04	0.09	0.19	0.01	0.08	0.01	0.65
	JAS	64.0	44.34	33.35	-0.62	-0.52	-0.04	0.1	0.1	0.03	0.52	0.44	0.08	0.0	0.0	0.1
CPS	AMJ	21.37	9.27	7.22	0.35	0.1	0.01	0.11	0.06	0.02	0.22	0.08	0.02	0.0	0.09	0.44
	JAS	79.86	37.28	18.87	0.41	0.15	0.1	0.15	0.1	0.04	0.17	0.06	0.19	0.01	0.15	0.01
S. Beaufort	AMJ	13.29	9.9	7.09	0.19	0.09	0.05	0.1	0.05	0.03	0.09	0.07	0.06	0.07	0.12	0.17
	JAS	22.38	16.78	11.17	0.34	0.14	0.12	0.14	0.07	0.04	0.15	0.1	0.19	0.02	0.06	0.01
N. Beaufort	AMJ	9.74	7.29	8.61	0.14	0.05	0.06	0.05	0.07	0.03	0.16	0.02	0.09	0.02	0.41	0.07
	JAS	21.12	18.05	13.38	0.29	0.27	0.14	0.11	0.15	0.04	0.17	0.09	0.26	0.01	0.08	0.0
S. Chukchi	AMJ	43.33	66.94	18.73	0.76	0.91	0.17	0.23	0.25	0.05	0.25	0.28	0.26	0.0	0.0	0.0
	JAS	114.96	161.37	28.91	1.18	0.65	0.15	0.32	0.52	0.05	0.28	0.04	0.2	0.0	0.22	0.01
N. Chukchi	AMJ	5.42	5.06	4.86	0.15	0.09	0.07	0.05	0.04	0.02	0.24	0.15	0.39	0.0	0.02	0.0
	JAS	16.25	13.55	8.86	0.15	0.13	0.07	0.1	0.09	0.03	0.06	0.06	0.11	0.17	0.17	0.05
S.E. Siberian	AMJ	50.31	83.42	23.87	0.9	1.02	0.34	0.3	0.33	0.09	0.21	0.22	0.29	0.01	0.0	0.0
	JAS	107.27	213.91	39.62	0.64	0.77	0.23	0.34	0.45	0.08	0.1	0.08	0.18	0.07	0.09	0.01
N.E. Siberian	AMJ	3.54	3.77	2.55	0.11	0.05	0.03	0.03	0.02	0.01	0.34	0.14	0.2	0.0	0.02	0.01
	JAS	9.48	6.96	4.36	0.1	0.12	0.05	0.04	0.04	0.01	0.14	0.22	0.32	0.03	0.0	0.0
Kara	AMJ	52.63	87.14	42.2	0.94	1.21	0.69	0.24	0.34	0.17	0.31	0.28	0.32	0.0	0.0	0.0
	JAS	88.79	175.88	69.53	0.27	-0.32	0.06	0.19	0.36	0.07	0.06	0.02	0.02	0.17	0.39	0.44
Barents	AMJ	305.39	438.88	91.53	1.9	1.89	0.4	0.6	0.7	0.13	0.23	0.18	0.21	0.0	0.01	0.01
	JAS	229.24	249.24	69.38	0.39	-0.25	0.06	0.31	0.26	0.06	0.04	0.03	0.04	0.22	0.36	0.27
North_of_66.5	AMJ	961.53	1118.59	383.66	7.17	5.43	2.27	1.26	1.5	0.41	0.49	0.28	0.48	0.0	0.0	0.0
	JAS	1093.61	1189.98	446.1	3.24	1.06	1.46	1.12	1.01	0.21	0.2	0.03	0.58	0.01	0.3	0.0

Table S3. Integrated phytoplankton concentration statistics per model

Statistics of integrated phytoplankton concentration integrated over the top 100 m of the water column for spring (AMJ) and summer (JAS). Units are in mmol-C m^{-3} (To obtain the total PP for the given quarter year, the value needs to be divided by 4). Indicated are mean, trend, standard deviation (STDEV), **R2 and p value from 1980 to 2015 for NAA-CanOE-CSIB, NAA-CMOC and NAA-PISCES.

Region	Season	Mean			Trend			StDev			R2			PValue		
		Canoe-CSIB	CMOC	PISCES	Canoe-CSIB	CMOC	PISCES	Canoe-CSIB	CMOC	PISCES	Canoe-CSIB	CMOC	PISCES	Canoe-CSIB	CMOC	PISCES
Arctic Basin	AMJ	0.09	0.23	0.34	0.0	0.0	0.0	0.0	0.0	0.0	0.47	0.1	0.32	0.0	0.07	0.0
	JAS	0.39	0.62	0.75	0.0	-0.0	0.0	0.0	0.0	0.0	0.07	0.01	0.2	0.13	0.51	0.01
Baffin Bay	AMJ	0.62	0.86	0.98	-0.0	-0.01	0.0	0.0	0.0	0.0	0.0	0.18	0.06	0.96	0.01	0.15
	JAS	0.76	1.24	1.0	-0.0	-0.01	-0.0	0.0	0.0	0.0	0.27	0.34	0.01	0.0	0.0	0.67
CPS	AMJ	0.17	0.24	0.38	0.0	0.0	0.0	0.0	0.0	0.0	0.21	0.1	0.1	0.01	0.06	0.07
	JAS	0.7	1.53	1.02	0.0	0.01	0.01	0.0	0.01	0.0	0.31	0.04	0.46	0.0	0.25	0.0
S. Beaufort	AMJ	0.64	1.91	1.06	0.01	0.02	0.0	0.0	0.01	0.0	0.07	0.07	0.05	0.12	0.13	0.19
	JAS	1.01	2.69	1.51	0.01	0.01	0.01	0.0	0.02	0.0	0.15	0.01	0.3	0.02	0.51	0.0
N. Beaufort	AMJ	0.12	0.24	0.44	0.0	0.0	0.0	0.0	0.0	0.0	0.14	0.02	0.18	0.02	0.44	0.01
	JAS	0.32	0.65	0.73	0.0	0.01	0.0	0.0	0.01	0.0	0.13	0.07	0.06	0.03	0.11	0.15
S. Chukchi	AMJ	0.49	2.12	0.84	0.01	0.03	0.01	0.0	0.01	0.0	0.28	0.26	0.35	0.0	0.0	0.0
	JAS	1.25	5.89	1.02	0.01	-0.0	0.0	0.0	0.02	0.0	0.25	0.0	0.09	0.0	0.87	0.08
N. Chukchi	AMJ	0.1	0.24	0.4	0.0	0.0	0.0	0.0	0.0	0.0	0.25	0.14	0.39	0.0	0.02	0.0
	JAS	0.38	0.96	0.69	0.0	0.01	-0.0	0.0	0.01	0.0	0.06	0.04	0.0	0.17	0.23	0.82
S.E. Siberian	AMJ	0.73	4.93	1.12	0.01	0.07	0.01	0.0	0.02	0.0	0.24	0.21	0.28	0.0	0.01	0.0
	JAS	1.46	14.68	1.51	0.01	0.01	0.0	0.0	0.03	0.0	0.11	0.0	0.05	0.05	0.74	0.2
N.E. Siberian	AMJ	0.15	0.54	0.47	0.0	0.01	0.0	0.0	0.0	0.0	0.32	0.2	0.2	0.0	0.01	0.01
	JAS	0.5	1.75	0.74	0.0	0.02	0.0	0.0	0.01	0.0	0.15	0.18	0.3	0.02	0.01	0.0
Kara	AMJ	0.63	4.18	1.23	0.01	0.06	0.01	0.0	0.02	0.0	0.35	0.29	0.33	0.0	0.0	0.0
	JAS	1.02	8.48	1.85	0.0	-0.04	-0.0	0.0	0.02	0.0	0.02	0.09	0.04	0.39	0.09	0.22
Barents	AMJ	1.5	8.33	1.25	0.01	0.03	0.0	0.0	0.01	0.0	0.23	0.11	0.18	0.0	0.04	0.01
	JAS	1.03	3.34	0.83	0.0	-0.01	-0.0	0.0	0.01	0.0	0.07	0.06	0.0	0.12	0.15	0.86
North_of_66.5	AMJ	0.6	2.35	0.74	0.0	0.01	0.0	0.0	0.0	0.0	0.51	0.23	0.61	0.0	0.0	0.0
	JAS	0.72	2.52	0.92	0.0	-0.0	0.0	0.0	0.0	0.0	0.37	0.02	0.47	0.0	0.37	0.0